https://doi.org/10.5194/acp-2019-900
Preprint. Discussion started: 7 November 2019

Predicting Secondary Organic Aerosol Phase State and Viscosity and its Effect on Multiphase Chemistry in a Regional Scale Air Quality Model

Ryan Schmedding[1], Quazi Z. Rasool[1*], Yue Zhang[1,4], Havala O. T. Pye [1,2], Haofei Zhang[3], Yuzhi Chen[1], Jason D. Surratt[1], Ben H. Lee[5], Claudia Mohr[5,8], Felipe D. Lopez-Hilfiker[5,9], Joel A. Thornton[5], Allen H. Goldstein[6,7] and William Vizuete[1€]*

1. Department of Environmental Science and Engineering, The University of North Carolina at Chapel Hill, Chapel Hill, North Carolina, 27516
2. National Exposure Research Laboratory, Office of Research and Development, Environmental Protection Agency, Research Triangle Park, Durham, North Carolina, 27709
3. Department of Chemistry, University of California at Riverside, Riverside, California, 92521
4. Aerodyne Research, Inc., Billerica, Massachusetts, 01821
5. Department of Atmospheric Sciences, University of Washington, Seattle, WA 98195
6. Department of Environmental Science, Policy, and Management, University of California, Berkeley, CA 94720
7. Department of Civil and Environmental Engineering, University of California, Berkeley, CA 94720
8. Present address: Department of Environmental Science and Analytical Chemistry, Stockholm University, SE-106 91 Stockholm, Sweden.
9. Present address: Tofwerk AG, CH-3600 Thun, Switzerland.

* Shared lead authorship

[€] Corresponding author: e-mail: vizuete@unc.edu; Telephone: +1 919-966-0693; Fax: +1 919-966-7911

Abstract

Atmospheric aerosols are a significant public health hazard and have substantial impacts on the climate. Secondary organic aerosols (SOA) have been shown to phase separate into a highly viscous organic outer layer surrounding an aqueous core. This phase separation can decrease the partitioning of semi-volatile and low-volatile species to the organic phase and alter the extent of acid-catalyzed reactions in the aqueous core. A new algorithm that can determine SOA phase separation based on their: glass transition temperature (T_g), Oxygen to Carbon ($O{:}C$) ratio, concentrations relative to sulfate concentrations; and meteorological conditions were implemented into the Community Multiscale Air Quality Modeling (CMAQ) System version 5.2.1 and was used to simulate the conditions in the continental United States for the summer of 2013. SOA formed at the ground/surface level was predicted to be phase separated with core-shell morphology i.e. aqueous inorganic core surrounded by organic coating, 68.5% of the time for continental United States. The phase states of organic coatings switched between semi-solid and liquid states, depending on the environmental conditions. The semi-solid shell occurring with lower aerosol liquid water content (western United States and at higher altitudes) has a viscosity that was predicted to be 10^2-10^{12} Pa•s which resulted in organic mass being decreased due to diffusion limitation. The organic phase was primarily liquid where aerosol liquid water was dominant (eastern United States and at surface), with a viscosity < 10^2 Pa•s. Phase separation while in a liquid phase state, i.e. Liquid-Liquid Phase Separation (LLPS), also reduces reactive uptake rates relative to homogenous internally mixed liquid morphology, but was lower than aerosols with thick viscous organic shell. The implementation of phase separation parameters in CMAQ led to a reduction of fine particulate matter ($PM_{2.5}$) organic mass, with a marginal change in bias and error (< 0.1 μg/m^3) compared to field data collected during the 2013 Southern Oxidant and Aerosol

Study. Sensitivity simulations assuming higher dissolution rate of isoprene epoxydiol (IEPOX) into the particle phase and the treatment of aerosol water content mitigated this worsening in model performance, pointing out the need to better constrain the parameters that govern phase state and morphology of SOA.

1 Introduction

Particulate matter (PM) is one of six criteria pollutants regulated by the United States Environmental Protection Agency's (EPA) National Ambient Air Quality Standards (NAAQS), established by the 1970 Clean Air Act. There are two categories of PM regulated by NAAQS: Fine PM ($PM_{2.5}$), with particle diameter less than 2.5 µm, and coarse PM (PM_{10}), with particle diameter up to 10 µm. PM has adverse effects on the global climate (Carslaw et al., 2013; Grandey et al., 2018; Lee et al., 2016; Regayre et al., 2015). $PM_{2.5}$ also represents a substantial public health risk due to its association with increased overall mortality, due to cardiorespiratory diseases (Hwang et al., 2017; Jaques and Kim, 2000; Zanobetti and Schwartz, 2009). It has been estimated that 20-60% of $PM_{2.5}$ are comprised of organic aerosols (OA) (Docherty et al., 2008). These pollutant species are either directly-emitted primary organic aerosols (POA), or secondary organic aerosols (SOA), which form when volatile organic compounds (VOCs) undergo chemical reactions that reduce their volatility to the point that they either partition into the aerosol phase (Zhang et al., 2007) or react heterogeneously with the existing particles (Riva et al., 2019). Studies have found that SOA tends to form the bulk of observed OA around the world (Nozière et al., 2015). The VOCs that form SOA may be either from biogenic or anthropogenic sources and can vary both spatially and temporally to areas as confined as the community level (Yu et al., 2014).

Recent studies have shown that SOA may phase-separate under certain atmospherically relevant conditions into different morphologies. These observations have included a "partially-engulfed" organic-inorganic morphology; an "island" morphology, where discrete pockets of SOA dot a larger inorganic particle; and a "core-shell" morphology, characterized by an organic rich outer "shell" and aqueous inorganic "core" (Freedman, 2017; O'Brien et al., 2015; Price et al., 2015; Renbaum-Wolff et al., 2016; Song et al., 2015, 2016; You et al., 2012; Zhang et al., 2015, 2018a). Pye et al. (2018) applied the Aerosol Inorganic-Organic Mixtures Functional groups Activity Coefficients (AIOMFAC) model (Zuend et al., 2008) to predict the thermodynamic favorability of phase separation in SOA using a box model and found that aerosols over the southeastern United States may be phase separated as frequently as 70% of the time. In other work, Pye et al. (2017) used the ratio of organic matter to organic carbon (OM:OC) and the ambient relative humidity (RH) to predict phase separation frequencies exhibiting a complex behavior, being more common in urban areas with low OM:OC at low RH, but higher phase separation frequencies in rural areas attributed to increasing OM:OC at low RH.

When aerosols form a core-shell morphology, experimentally observed viscosities of the outer organic-rich shell and inner electrolyte-rich core have been shown to differ by up to three orders of magnitude resulting in possible diffusion limitations on reactive uptake (Ullmann et al., 2019). It has also been shown that the viscosity and subsequently diffusivity of the organic phase (D_{org}) may vary as a function of SOA composition (Grayson et al., 2017). Laboratory experiments have been conducted to measure the viscosity of SOA using poke-flow and bead mobility techniques (Reid et al., 2018; Renbaum-Wolff et al., 2013; Song et al., 2015, 2016). These studies have found that SOA formed from anthropogenic precursors, such as benzene, toluene, and xylene, have similar D_{org} values in the realm of 10^{-14}-10^{-16} m^2/s (Grayson et al., 2016; Song et al., 2015, 2016, 2018). Similar studies on biogenic SOA comprised of α-pinene oxidation products, however found that its measured viscosities and calculated diffusion coefficients are lower than those of anthropogenic SOA by as much as 2 orders of magnitude at comparable conditions (Song et al., 2016, 2018; Zhang et al., 2015).

The most abundantly emitted biogenic VOC is isoprene (2-methyl-1,3-butadiene) with average annual global emissions totaling to approximately 500-750 Tg-C yr^{-1} (Guenther et al., 2006; Liao et al., 2015). Isoprene is known to react with hydroxyl (OH) radicals under low-NO$_x$ (=NO+NO$_2$) conditions to form isoprene hydroxyhydroperoxides (ISOPOOH) (Jacobs et al., 2014; Krechmer et al., 2015). If the reaction pathway continues with OH, ISOPOOH will react again to form isoprene epoxydiol (IEPOX) (Bates et al., 2014; Paulot et al., 2009; Surratt et al., 2010). It is possible for IEPOX to form products with sufficiently low volatility to form SOA via a reactive uptake pathway onto acidified sulfate seed particles (Bondy et al., 2018; Surratt et al., 2006, 2007, 2010). IEPOX-derived SOA have been observed to account for up to 36% of biogenic SOA in the southeastern United States during the summer (Budisulistiorini et al., 2016). Given the importance of this pathway there has been increased focus on the phase state of particles and its impact on reactive uptake (Budisulistiorini et al., 2017).

Prior measurements of isoprene-derived SOA suggested that it would not be viscous enough to exhibit diffusion limitations; however, there is much uncertainty with these measurements as those particles mainly formed through nucleation of semi-volatile species (Song et al., 2015). IEPOX-derived SOA that specifically account for up to one-third or more of total organic aerosol mass in southeastern United States has shown to exhibit higher volatility than the remaining bulk, but IEPOX-derived SOA does have a low volatility (Lopez-Hilfiker et al., 2016). However, IEPOX heterogeneous reaction pathways that typically happen in the ambient conditions lead to formation of organosulfates that have potentially higher viscosities (Riva et al., 2019). Furthermore, RH (Huang et al., 2018; Pajunoja et al., 2014; Song et al., 2015, 2016; Zhang et al., 2015, 2018a), temperature (Maclean et al., 2017), degree of oligomerization , and mass loading (Grayson et al., 2016) also impact particle viscosity. Higher RHs may result in more water to partition into the particle and act as a plasticizer which decreases its viscosity (Song et al., 2015, 2016, 2018; Zhang et al., 2011). Higher temperatures also increase the diffusion coefficient (Chenyakin, 2015). Degree of oligomerization increases the viscosity of SOA and therefore reduce its $D_{org.}$ as well (Grayson et al., 2017). The competing sinks between heterogeneous reactions and losses of semi-volatile gas species also amplify the effects of phase state on aerosol formation (Zhang et al., 2018a). The experimental data provided from previous studies highlight the urgency of incorporating those results into regional and global models to predict the effects of phase states in aerosol formation in the ambient environment accurately. A recent study by Schmedding et al. (2019) used a dimensionless (0D) box model for phase-separated SOA formation at the Look Rock Site during the 2013 Southern Oxidant and Aerosol Study (SOAS). Our prior work found that the inclusion of a phase-separation parameter could either inhibit SOA due to diffusion limitations in the separated organic phase or increase it by concentrating the electrolytes into the aqueous core leading to faster acid-catalyzed reactions. This resulted in decreasing normalized mean error (NME) of the model from 83.4% to 77.9% and the normalized mean bias (NMB) from -66.2% to -36.3% compared to a previous work simulating the same dataset that assumed homogenous aerosol (Budisulistiorini et al., 2016). Our previous model study (Schmedding et al., 2019) highlighted the significant impact of an organic coating layer on IEPOX-derived SOA formation, but lacked any quantification of conditions that result in phase separation creating such organic coating and its phase state.

The inclusion of an explicit reaction pathway for the reactive uptake of acid-catalyzed IEPOX-derived SOA in both regional and global scale chemical transport models (CTMs), such as the Community Multi-Scale Air Quality Model (CMAQv5.2.1) and the Goddard Earth Observing System (GEOS-Chemv11-02-rc), have substantially improved the performance of predicted SOA yields (Marais et al., 2016; Pye et al., 2013; Pye et al., 2017). These models do not include parameters in their aerosol algorithms that account for aerosol phase separation and its impact on SOA formation (Marais et al., 2016; Pye et al., 2017, 2018), which can lead to potential deviations of aerosol quantification. This work systematically examines when coatings comprised of OA derived from a mixture of biogenic and anthropogenic compounds are formed (i.e. predicting phase separation frequencies and how coatings impacts SOA formation from acid-catalyzed multiphase reactions of IEPOX) by implementing parameterizations to determine the viscosity and phase-state of particles (liquid or glassy) in CMAQ and simulating for the continental United States.

2 Methods

2.1 Phase state and its impact on reactive uptake: overview

Organic constituents of an aerosol exhibit a solid-like glassy phase when the ambient temperature is below the glass transition temperature (T_g), which is a function of RH and the aerosol composition (DeRieux et al., 2018). A liquid phase occurs when the T_g is lower than ambient temperature. The difference in viscosity (η_{org}) of organic-rich phase of aerosol, below and above the T_g, may be as high as 8 orders of magnitude (Marsh et al., 2018). The T_g can determine when aerosols are in a highly viscous glassy state ($\eta_{org} \geq 10^{12}\ Pa \bullet s$), a semisolid state ($100 \leq \eta_{org} < 10^{12}\ Pa \bullet s$), or in a liquid state ($\eta_{org} < 100\ Pa \bullet s$) (Marcolli et al., 2004; Martin, 2000). Aerosols in a highly viscous or a semisolid state are assumed to be phase separated as a model simplification (refer to Section 2.3). This simplification is based on recent observations showing higher than anticipated rebound fractions (i.e., almost full resistance to reactive uptake) attributed to organic aerosol constituents with viscosities > $10^2\ Pa \bullet s$. These aerosols were phase separated having an amorphous solid coating, which, unlike liquid particles, can only dissipate energy by rebounding (Bateman et al., 2015a, 2015b, 2017; Reid et al., 2018; Virtanen et al., 2010). Aerosols that are in a liquid state may either be an internal homogenous mixture, or they can also be phase separated known as liquid-liquid phase separation (LLPS). The occurrence of LLPS depends on the average O:C ratio, organic mass to sulfate ratio, ambient temperature and ambient RH (Song et al., 2018; Zuend and Seinfeld, 2012). In addition, a sensitivity case was completed where it was not assumed that a semisolid state is always phase-separated, and instead the LLPS criteria was applied for conditions that produce a low aerosol water content (refer to Section 2.6).

Phase state of an organic shell impacts reactive uptake by affecting the diffusivity of a species through this outer organic phase (D_{org}). D_{org} can be related to the viscosity of the organic phase (η_{org}) using the Stokes-Einstein Equation, as shown in Eq. (1) (Ullmann et al., 2019):

$$D_{org} = \frac{k_b T}{6\pi \eta_{org} r_{diffusive}} \qquad (1)$$

Where k_b is the Boltzmann constant, T is the ambient temperature, η_{org} is the organic phase viscosity, and $r_{diffusive}$ is the hydrodynamic radius of the molecule diffusing through the viscous organic phase.

2.2 Determining the Glass Transition Temperature (T_{org})

The combined T_{org} for anthropogenic and biogenic species and aerosol water associated with them was found using a modified version of the Gordon-Taylor Mixing Rule, as represented in Eq. (2) (DeRieux et al., 2018; Gordon and Taylor, 1952):

$$T_{org} = \frac{\left(w_s T_{g,w} + \frac{1}{k_{GT}}\left(w_a T_{g,a} + w_b T_{g,b}\right)\right)}{w_s(RH) + \frac{1}{k_{GT}}(w_a + w_b)} \qquad (2)$$

where $T_{g,w}$ is the glass transition temperature of water (*137 K*) (Koop et al., 2011). $T_{g,a}$ and $T_{g,b}$ are the respective glass transition temperatures (*K*) for the anthropogenic (also includes all combustion-generated POA in addition to VOC-derived SOA, see Table 1) and biogenic (only includes VOC-derived SOA, see Table 1) fractions of OA. K_{GT} is the Gordon-Taylor constant, which is assumed to be 2.5 based off of Koop et al., (2011). w_a and w_b are the mass fractions of anthropogenic and biogenic OA species, respectively. $w_s(RH)$ or simply w_s is the mass fraction of organic aerosol water.

For this work, it was assumed that 10% of the aerosol water was present in the organic phase, within the range of organic water reported by Pye et al. (2017). In CMAQv5.2.1, the total aerosol water, 10% of which is directed to the organic phase, is predicted by ISORROPIA and only associated with inorganic electrolytes such as, ammonium bisulfate (Pye et al., 2017). As represented in Eq. (3), the w_s along with the w_a and w_b make up the organic-water component of the aerosol and adds up to 1:

$$w_s = 1 - (w_a - w_b) \tag{3}$$

Shiraiwa et al. (2017) used 179 organic species to fit a relationship between T_g, the molar mass (M), and O:C ratio (Shiraiwa et al., 2017) . Following the same relationship as in Eq. (4), the respective glass transition temperatures for the anthropogenic and biogenic fractions ($T_{g,a}$ and $T_{g,b}$, also referred as, T_{biog} *and* T_{anth}) were calculated using the weighted average molar mass (M_x) and O:C ratio ($(O{:}C)_x$) for all individual anthropogenic and biogenic species addressed in CMAQ (see Table 1). Where, x refers to *a - anthropogenic OA (anth) or b- biogenic OA (biog);* i refers to individual species:

$$T_{g,x}\ or\ T_x = -21.57 + 1.51M_x - 0.0017M_x^2 + 131.4(O{:}C)_x - 0.25M_x(O{:}C)_x \tag{4}$$

$$Where, M_x = \sum(w_{i,x} * M_{i,x})\ ;\ O{:}C_x = \sum(w_{i,x} * O{:}C_{i,x})\ ;\ w_{i,x} = \frac{Mass\ Concentration_{i,x}}{Total\ Mass\ Concentraion_x}$$

When the ambient temperature is below the T_{org}, the viscosity of the coating (η_{org}) is assumed to remain constant at $10^{12}\ Pa \bullet s$. When the ambient temperature is greater than or equal to the calculated T_{org}, the viscosity of the organic phase is calculated using a modified Vogel-Tamman-Fulcher Equation (DeRieux et al., 2018; Fulcher, 1925; Tamman and Hesse, 1926; Vogel, 1921) as shown in Eq. (5) with experimentally fitted parameters as shown in Eqs. (6) and (7):

$$log_{10}(\eta_{org}) = -5 + 0.434\frac{T_0 D}{T - T_0} \tag{5}$$

$$T_0 = \frac{39.17T_{org}}{D + 39.17} \tag{6}$$

$$D = 14.4 - 2.3(O:C)_{avg} \tag{7}$$

T is the ambient temperature (K), T_0 is an experimentally fitted parameter of Eq. (5) that varies as a function of T_{org} and the fragility parameter D, which is a function of the O:C ratio (DeRieux et al., 2018; Zhang et al., In Prep). $O:C_{avg}$ refers to the overall OA (including both POA- all anthropogenic and SOA- anthropogenic and biogenic, see Table 1) O:C ratio given by CMAQ.

The effective diffusion coefficient for IEPOX through the organic coating (D_{org}) was then calculated using the Stokes- Einstein Equation (refer to Eq. (1)), assuming that $r_{diffusive}$ = 1 nm (Evoy et al., 2019; Ullmann et al., 2019).

2.3 Phase Separation

SOA phase state was determined by multiple criteria. As a model simplification, any SOA was considered to be semisolid –phase separated (SSPS) when $\eta_{org} > 100$ Pa•s ($T_{org}:T \geq 0.8$) based on Shiraiwa et al., (2017) as shown in Figs. 1 and 4A. LLPS occurs for aerosols with $\eta_{org} \leq 100$ Pa•s ($T_{org}:T < 0.8$) when RH ≤ separation relative humidity (SRH_{LLPS}). Song et al. (2018) suggests that LLPS always happens when $(O:C_{avg}) \leq 0.56$, which we implemented to predict phase separation along with conditions specified for $(O:C_{avg}) > 0.56$ in Eqs. (8) and (9). The SRH_{LLPS} is dependent on OA composition as shown in Eqs. (8) and (9) based on Bertram et al. (2011), Zuend and Seinfeld (2012) and Song et al. (2018):

$$SRH_{LLPS} = 35.5 + 339.9(O:C_{avg}) - 471.8\,(O:C_{avg})^2 \tag{8}$$

$$when\ 0.56 < (O:C_{avg}) \leq 0.73\ and$$

$$0.1 < (OM : Inorganic\ Sulfate) \leq 15$$

$$SRH_{LLPS} = 0 \qquad i.e. no\ LLPS \qquad (9)$$

$$when\ (O{:}C_{avg}) > 0.73\ and$$

$$0.1 < (OM : Inorganic\ Sulfate) \leq 15$$

2.4 Model description and implementation

All simulations were completed in CMAQv5.2.1 for the SOAS campaign from June 1 - July 15, 2013, with ten days of spin-up time starting on May 21, 2013. Model inputs are described in Xu et al. (2018). The horizontal resolution of the simulation was 12km x 12km. Model vertical extent between the surface and 50 hPa (representing possible stratospheric influences) consisted of 35 layers of variable thickness. Weather Research and Forecasting model (WRF) Advanced Research WRF (ARW) version 3.8 with lightning assimilation was used to generate the meteorological inputs for the simulations (Appel et al., 2017; Heath et al., 2016). The National Emission Inventory (NEI) 2011 v2 produced by the EPA was used to generate anthropogenic emissions. Biogenic emissions were determined using the Biogenic Emission Inventory System (BEIS) v3.6.1 (Bash et al., 2016). BEIS predicts lower emissions amounts for isoprene than the Model of Emissions of Gases and Aerosols from Nature (MEGAN) (Carlton and Baker, 2011). Therefore, emissions of isoprene were increased in this work to 1.5x their original levels based on Pye et al. (2017) who found that this increase led to better agreement with field measurements of isoprene and OH at the Centreville site during the 2013 SOAS. Carbon Bond v6.3 (CB6r3) was used for the gas-phase chemistry in the model (Emery et al., 2015; Hildebrant Ruiz and Yarwood, 2013; Yarwood et al., 2010).

2.5 Reactive Uptake

IEPOX-derived SOA is modeled with a first-order heterogeneous uptake reaction that includes a new term that accounts for diffusion limitations due to an organic coating when the aerosol phase state demands it, as described below in Eqs. (10)-(13) (Anttila et al., 2006; Gaston et al., 2014; Ryder et al., 2014; Budisulistiorini et al., 2017). The impact of organic coating was not considered in the original IEPOX reactive uptake algorithm in CMAQ (Pye et al., 2013):

$$IEPOX_{(g)} \rightarrow IEPOXSOA_{(aerosol)} \qquad (10)$$

This first-order heterogeneous-reaction rate constant (k_{het}) is defined as:

$$k_{het} = \frac{SA}{\frac{r_p}{D_g} + \frac{4}{v\gamma}} \qquad (11)$$

Where SA is the aerosol surface area *($\mu m^2/m^3$)*, v is the mean molecular speed *(m/s)* of gas phase IEPOX estimated by Eq. (12):

$$v = \sqrt{\frac{8*R*T}{\pi*MW_{IEPOX}}} \qquad (12)$$

r_p is the effective molecular particle radius including both the inorganic core and organic shell *(m)*, D_g is IEPOX diffusivity in the gas phase ($1.9 * (MW_{IEPOX})^{-\frac{2}{3}} \frac{m^2}{s}$), MW_{IEPOX} = 118 g mol^{-1} is the molecular weight of IEPOX and γ is the reactive uptake coefficient:

$$\frac{1}{\gamma} = \frac{1}{\alpha} + \frac{v*r_p^2}{4H_{inorg}*R*T*D_a*r_{core}} \frac{1}{q*coth(q)-\frac{1}{q}} + \frac{v*l_{org}*r_p}{4*H_{org}*R*T*D_{org,eff}*r_{core}} \qquad (13)$$

α is the accommodation coefficient (0.02). H_{inorg} is the Henry's Law coefficient into the inorganic phase ($3 * 10^7 \frac{M}{atm}$). R is the gas constant ($0.08026 \frac{L*atm}{K*mol}$), T is the ambient temperature (K).

D_a is the IEPOX diffusivity in the aerosol core $(10^{-9}\frac{m^2}{s})$ and q is the diffuso-reactive parameter as defined in Eq. (13):

$$q = \mathrm{r_p}\sqrt{\frac{\mathrm{k_{particle}}}{\mathrm{D_a}}} \tag{14}$$

$k_{particle}$ is the pseudo-first order rate constant (s^{-1}) defined in Eq. (14) (Pye et al., 2013), with parameters defined in Table 2:

$$k_{particle} = \sum_{i=1}^{N}\sum_{j=1}^{M} k_{i,j}\,[nuc_i][acid_j] \tag{15}$$

$D_{org,eff}$ $(\frac{m^2}{s})$ is the effective diffusivity of IEPOX through an organic coating compromised of the species given in Table 1 and 10% of the total aerosol liquid water.

The contribution of organic species to the volume of the core is assumed negligible and water moves freely between the inorganic core and the organic shell, leading to approximately 90% aerosol water in inorganic core and 10% in the organic shell for this work as described by Pye et al. (2017). An extension of this assumption is that the inorganic ion species are concentrated entirely within the aqueous core when calculating $k_{particle}$. H_{org} $(2 * 10^5\ M/atm)$ is the effective Henry's Law constant for the organic coating and l_{org} is the organic phase thickness given by Eq. (16) calculated at each time step based off of Riemer et al. (2009). r_p is the surface-area weighted median particle radius based on surface area distribution of different species and β is the ratio of inorganic particle volume (90% of the particle water and inorganic species) to the total particle volume (all organic species, water, and inorganic species):

$$l_{org} = r_p(1-\beta^{\frac{1}{3}}) \tag{16}$$

https://doi.org/10.5194/acp-2019-900
Preprint. Discussion started: 7 November 2019

r_p is the effective aerosol radius (m) same as in Eqs. (11), (13) and (14), and r_{core} is the aerosol inorganic core radius (m). r_{core} is defined based off of Riemer et al. (2009) below:

$$r_{core} = r_p \beta^{\frac{1}{3}} \qquad (17)$$

Particles that did not have LLPS or SSPS morphology were assumed to form a homogenous mixture of organics and inorganics (i.e. $l_{org} = 0$), reducing Eq. (13) to the standard CMAQ treatment.

2.6 Sensitivity simulations

A sensitivity simulation (*Emission Reduction*) was conducted using the EPA's emission reductions estimates of 34% and 48% for NO_x and SO_2, respectively, from 2013 to 2025 (Marais et al., 2016; Eyth et al., 2014). A second sensitivity (*HighHorg*) was conducted that used the same upper bound of H_{org} as reported by Schmedding et al. (2019) increasing the value from $2*10^5$ M/atm to $3*10^8$ M/atm. To better understand the effects of viscosity on particle morphology and phase separation, a third sensitivity simulation (*PhaseSep2*) was conducted where the phase separation of particles was determined solely by Eqs. (8) and (9). This simulation excluded the erstwhile criteria that particles with $\eta_{org} > 100$ Pa•s were automatically phase separated with a semi-solid outer core, also referred as SSPS morphology. Table 3 gives a brief description of the *NonPhaseSep* simulation (base CMAQ without phase state and organic coating impacts), the new *PhaseSep* proposed in this work, and the three sensitivity simulations: *Emissions Reductions*, *HighHorg*, and *PhaseSep2*.

2.7 Measurement Comparisons

Field data were collected using a high-resolution time-of-flight chemical ion mass-spectrometer (HTOF-CIMS) coupled with a filter inlet for gases and aerosols (FIGAERO) and a two-dimensional gas chromatogram time-of-flight mass spectrometer (GC×GC-TOFMS) at the Centreville, AL site during the 2013 SOAS campaign (Zhang et al., 2018b). The combined measurements provide comprehensive and quantitative molecular compositions of over 800 OA species with a time resolution of 4 hours. Chemical formulas were assigned to all the species based on high-resolution peak fitting and hence their O:C ratios and molecular weights are known, which were then used to empirically calculate the average T_{org} of the OA at the site for the duration of the entire SOAS campaign (June 1- July 15, 2013). The speciated OA were estimated to account for 74% of total fine OA mass during SOAS. The uncharacterized fraction of fine OA (e.g., organosulfur compounds) will likely have some influence on the estimated T_{org}. Also note that both techniques use thermal desorption approach to analyze OA composition which was recently shown to cause thermal decomposition for certain species (Lopez-Hilfiker et al., 2016; Cui et al., 2018). Thus, some interferences in T_{org} estimation could be expected by thermal decomposition; however, at this time it remains unclear how substantial these interferences could be due to lack of understanding of the degree of decomposition that occurs in these analytical methods. Nevertheless, to our knowledge, this is the most comprehensive molecular-level OA speciation data set, and thus, is appropriate to use for comparison with modeled T_{org} in this work.

Model simulation results (*PhaseSep, HighHorg* and *PhaseSep2*) were compared to recorded values for $PM_{2.5}$ organic carbon mass concentration at monitoring stations that are a part of the

South Eastern Aerosol Research Characterization study (SEARCH) (Hansen et al., 2003) to better constrain the parameters used in the calculation γ_{IEPOX}.

3 Results

3.1 Predicted Aerosol Phase State

The ratio of T_{org} to the ambient T is the strongest indicator of the phase state of the aerosol. The mean value for T_{org} for all grid cells on the surface level and for all time steps was 207 K with a maximum value of 284 K, a minimum value of 137 K, and a median of 223 K. The values of T_{biog} and T_{anth} ranged from 160-301 K and 230-311 K, respectively. This indicates that anthropogenic species have a higher range of glass transition temperatures than biogenic species; however, the maximum values of T_{biog} and T_{anth} are relatively closer than their minimum values. This is attributed to the abundant biogenic acid-catalyzed IEPOX-derived SOA species, such as organosulfates and 2-methyltetrols, having a high T_g of 301 K and a viscosity of 10^{12} as shown in Table 1. An Analysis of variance (ANOVA) test was completed to determine if T_{org}, T_{biog}, and T_{anth} were significantly different ($p < 2*10^{-16}$). It was found that the aforementioned three categories of glass transition temperatures were statistically different from each other.

For the simulation period, the diurnal variability (i.e., between day and night) in the ambient T at any site was ~10 K, while T_{org} varied by as much as 75 K within a 24-hour period. This indicates that changes in the T_{org}:T ratio (i.e. Phase state) were driven by T_{org} (i.e., composition of the organics-water system) rather than T.

Figure 1 gives the predicted probability density distribution of the T_{org}:T ratio at the surface level of CMAQ for all grid cells and time steps. At the surface the range of T_{org}:T ratios was from 0.455 to 0.987 with a median value of 0.763 and a mean value of 0.703. In the surface layer over 63.5% of the T_{org}:T ratios were less than 0.8, a value which is given as the transition point from a semi-solid viscosity to a liquid-like viscosity (Shiraiwa et al., 2017), while the other 36.5% of the condition that the T_{org}:T were more than 0.8, indicating the aerosols were in semi-solid phase state. Also shown in Figure 1 are the T_{org} :T ratio at the 18th layer (~ 1.8 km above ground level), 28th layer (~ 8 km above ground level) and the 35th layer (~ 17 km above ground level). For 18th layer (i.e., lower troposphere), T_{org}:T ratios ranged from 0.464 to 1.022 with a median value of 0.807 and mean value of 0.772. For 28th layer (i.e., upper troposphere), T_{org}:T ratios ranged from 0.523 to 1.201, with a median value of 0.890 and mean value of 0.892. For 35th layer (i.e., stratosphere), T_{org}:T ratios ranged from 0.901 to 1.37, with a median value of 1.114 and mean value of 1.131. The frequency of liquid-like viscosity based on the T_{org}:$T < 0.8$ cut-off reduced to 47.31% for 18th and 0% for 35th layer eventually. Similarly, frequency of semi-solid or glassy particles based on the T_{org}:$T \geq 0.8$ cut-off increased to 52.69% for 18th, 84.38% for 28th and 100% for 35th layers eventually.

Figure 2A shows a map of the average surface layer T_{org}:T ratio across the Continental United States for the duration of the simulation. The T_{org}:T ratios exhibited a bimodal distribution both at the surface (Fig. 1 and Fig. 2A) and in the lower troposphere (Fig. 2B), where particles over the oceans had substantially higher w_s, driving down their T_{org}:T ratio. Semi-solid particles with a higher range of T_g values (Fig 2A) were concentrated over areas associated with higher anthropogenic SOA (including anthropogenic POA listed in Table 1) and a low RH, aerosol liquid

https://doi.org/10.5194/acp-2019-900
Preprint. Discussion started: 7 November 2019

water content, and biogenic SOA (i.e., the American southwest and Rocky Mountains). These higher T_g values pulled the net T_{org} value up closer to the ambient temperature, and thus, brought the T_{org}:T ratio closer to 1. The particles with the lowest T_{org} :T ratios were located over the Atlantic and Pacific oceans, due to the substantially higher aerosol water content and low levels, or even lack of anthropogenic and biogenic organics in these environments.

Figures 2B, 2C and 2D show the spatial profiles of the mean T_{org}:T ratio for each grid cell at the 18th layer of CMAQ (lower troposphere), 28th layer of CMAQ (upper troposphere) and the 35th layer of CMAQ (stratosphere). The value of T drops with the decreasing pressure. The O:C ratio of the particles are predicted to increase when compared to the surface due to atmospheric oxidation. The mean O:C ratio at the surface was 0.73, while across the troposphere (at layers 18 and 28) it was 0.75, and at layer 35 it was 0.77. The mean value of T_{org} also increased from 207 K at the surface to 219 K at layer 18, 223.5 K at layer 28 and 239 K at layer 35. This change in T_{org} was primarily driven by decreases in organic water in the aerosol. The mean concentration of water associated with organics (w_s) at the surface was 29%. At layer 18, this concentration was 17%, at layer 28 it was 11.5% and at layer 35 it was 1.4%. The removal of water from the organic phase led to the disappearance of the bimodal T_{org} :T ratio beyond the 28th layer (upper troposphere). The mean T_{org} :T ratio was less than 1 for all grid cells at the 18th layer (lower troposphere), and 59.7% of particles were likely to be liquid based on the T_{org}:T ratio < 0.8. The remaining 40.3% of particles were semi-solid because their T_{org} :T values were between 0.8 and 1. Semi-solid particles were still concentrated over the American southwest and Rocky Mountains. At the 18th layer (upper troposphere), 69.35% of the particles were semi-solid with T_{org}:T ratio between 0.8 and 1, with 15.61% and 15.03% of particles likely to be liquid (T_{org}:T ratio < 0.8) and solid (T_{org}:T ratio

> 1). At the 35th layer of CMAQ, all particles had a $T_{org}:T$ ratio > 1, indicating that the organic phases of all of the particles had glassy viscosities. By layer 35 (stratosphere), the particles mostly exhibit a solid-like behavior across the Continental United States. Particles with the highest $T_{org}:T$ ratio at this altitude were located over the southern half of the simulation area, with $T_{org}:T$ ratios approaching 1 in the northern half of the simulation. Particles in the Northern half of the Continental United States domain had higher concentrations of biogenic and anthropogenic SOA in comparison to those in the southern half of the domain and therefore had higher T_{org} values than their southern counterparts had.

Figure 3 is an illustrative example through model data extracted for June 1 - June 15, 2013, at two SEARCH monitoring sites. Figure 3 shows the diurnal profile and relative contributions of the model predicted anthropogenic, biogenic and water fractions to T_{org} for a rural site in Centreville, Alabama (Fig. 3A) and at an urban site at the Jefferson Street, Atlanta, Georgia (Fig. 3B). Both Centreville and Atlanta sites (Fig. 3) had T_{org} values that ranged from 175-250 K (Fig. S1). The Centreville site, however, is rural and the T_{org} is more dominated by biogenic emissions (Fig. 3A). Whereas, the Jefferson Street site has a significant contribution by both anthropogenic and biogenic emissions, but anthropogenic dominating slightly (Fig. 3B). Fig. S1 gives the diurnal pattern of relative contribution of aerosol liquid water to T_{org}. The peaks in T_{org} coincided with the daytime period of high emissions of VOCs and lower contribution of aerosol liquid water (Figs. 3 and S1). At night, due to higher contribution of aerosol liquid water, T_{org} is lower than daytime for both the sites (Fig. S1). Figure 3B shows that T_{org} at the Jefferson Street, Atlanta, Georgia has similar peaks, but a higher minimum value during the night, due to the higher budgets of anthropogenic VOCs or combustion-generated anthropogenic POA as compared to biogenic. Both sites have a relatively high contribution of aerosol water (generally true for eastern United States, see Fig. 2A) to the organic phase, especially at night for 18:00-8:00 local day hours (Fig. S1).

3.1.1 Predicted Viscosity

The abundance of water relative to organics (Fig. 4F) drives the model predicted variability in viscosity and phase separation. Whether a particle is semi-solid, or liquid, and whether it is in a LLPS state is influenced by the proportion of SOA constituents, including uptake of water by them and has implications for the organic-phase viscosity. Figures 4D-F show that, w_s (i.e., water related to organic phase) had the strongest correlation with η_{org} (r = 0.919) followed by w_b (r = 0.736) and w_a (r = 0.620) (i.e., biogenic and anthropogenic constituents in the organic phase, respectively). Figure 4A gives the probability density distribution of η_{org} at the surface level for all grid cells and time steps. The predicted viscosity for *PhaseSep* simulation ranged from $5.94*10^{-3}$ Pa•s to $5.31*10^{11}$ Pa•s with a mean value of $8.45*10^{5}$ Pa•s (median of 343 Pa•s). As shown in Figure 4A, the overall phase separation frequency was 68.5%, where 54.8% of predicted viscosities were greater than 100 Pa•s, indicating that they exhibited SSPS morphology. The mean of η_{org} of SSPS particles was $1.54*10^{6}$ Pa•s, and the median was $7.79*10^{3}$ Pa•s. The remaining 13.7% of the phase-separated particles exhibited a LLPS morphology. The median viscosity of LLPS particles was 1.14 Pa•s with a mean of 14.2 Pa•s with a range of $7.86*10^{-3}$ to 99.99 Pa•s. Ambient RH was also more strongly correlated with η_{org} (r = 0.677) than O:C ratio (r = 0.62) (Fig. 4B-C). $D_{org,eff}$, which is inversely related to η_{org} as derived from Eq. (1), had a range $1.20*10^{-24}$ m^2/s to $3.58*10^{-11}$ m^2/s and a mean and median of $3.40*10^{-12}$ m^2/s and $3.94*10^{-11}$ m^2/s, respectively. The mean O:C ratio was 0.678, with a range of 0.101 to 0.730. The mean fraction of the organic phase composed of water (w_s) was 42.4% with a range of $1.04*10^{-4}$ to 99.9%. The mean values of w_b and w_a in LLPS were 19.8% and 37.7%, respectively, with ranges of $1.76*10^{-5}$ to 82.1% and $2.15*10^{-5}$ to 96.9%. This suggests that anthropogenic aerosol components are likely more water soluble than biogenic components.

3.1.2 Comparison to Observed data

Figure 5 shows the T_{org}:T ratio calculated from speciated organic aerosol composition field data at the Centreville, Alabama field site (Zhang et al., 2018b) during the 2013 SOAS period. T_{org}:T ratio derived from data collected by Zhang et al. (2018b) ranged from 0.630 to 0.881. Also shown in Fig. 5 are the predicted T_{org}:T ratios using the phase separation (*PhaseSep*) parameterization. CMAQ modeled T_{org}:T ratio using *PhaseSep* simulation ranged from 0.531 to 0.902, slightly exceeding the range predicted from observations. It should be noted that the Zhang et al. (2018b) observations were recorded every four hours for ~ 60% of the 2013 SOAS time period. Modeled T_{org}:T mostly captures the peaks and drops, which the observation derived T_{org}:T shows (Fig. 5). Some mismatch can be attributed to the lack of an explicit mechanism to compute organic aerosol water uptake and some unaccounted SOA formation mechanisms. Further, Zhang et al. (2018b) only accounted for ~ 70% of SOA species listed in Table 1. During this time period the model had a normalized mean bias (NMB) of 2.37% when compared to observationally calculated values. Median and mean T_{org}:T ratios predicted from the 2013 SOAS field observations of 0.799 and 0.773, respectively, were quite close to the corresponding values of 0.784 and 0.769 predicted by PhaseSep simulation in CMAQ. The difference in observed and model estimated T_{org}:T range was statistically significant with a P-Value = 0.001, and a correlation coefficient of ~ 0.66 between them. There is also a discernable consistent diurnal trend across the 2013 SOAS period for T_{org}:T, such as stronger contribution of aerosol liquid water for 18:00-08:00 hours and a lowering of the T_{org}:T during those hours (Fig. 3A and S1).

Figure 6 shows the predicted viscosity of our phase separation implementation for all days, grid cells and layers sorted into 10% RH bins. The trends in range of modeled η_{org} are the same as in Fig. 4B, with narrower ranges at lower RH and wider ranges with increasing RH. Wider η_{org} ranges at higher RH can be explained by increased diffusivity with higher aerosol liquid water in SOA causing quick mixing times often accompanied with drastic differences in composition. Also, shown in Fig. 6 are viscosities of aerosols made in the laboratory. The red dots represent the viscosities of α-pinene SOA measured by Zhang et al. (2018a), and the blue box plots represent the range of viscosities of toluene SOA measured by Song et al. (2016). Both laboratory-based experimental studies show good agreement at atmospherically-relevant RH ranges with the viscosities predicted by our implementation. At lower RH ranges (~ 30%), the experimentally measured viscosities are slightly higher than those predicted by our study. This can be attributed to shattering of highly viscous SOA ($\eta_{org} \geq 10^6$ Pa•s) for RH ≤ 30% that inhibits their flow in laboratory measurements of η_{org} (Renbaum-Wolff et al., 2013; Zhang et al., 2015; Zhang et al., 2018a).

3.2 Impact on Model predictions

3.2.1 Reactive uptake coefficient of IEPOX (γ_{IEPOX})

Previous experimental studies show that phase separation forming semi-solid organic aerosol coatings is expected to decrease IEPOX reactive uptake (γ_{IEPOX}), and thus, the resulting SOA (Zhang et al., 2018a). Figure 7A shows reductions in γ_{IEPOX} with *Emission Reduction* sensitivity case subsequently reducing SOA (Fig. 10A), in agreement with recent modeling predictions that show emission reductions expected by 2025 lead to reductions in IEPOX SOA (Marais et al., 2016). This study implemented the phase separation and the phase separation parameters into CMAQ (*PhaseSep*), showing agreement with the previous experimental work (Zhang et al., 2018a), with the mean value of γ_{IEPOX} decreasing to 1.141*10^{-3} or a 18.3% decrease at the surface level, compared to 1.397*10^{-3} in original CMAQ with no phase separation considered (*NonPhaseSep*) (Fig. 7A). Similarly, the median value of γ_{IEPOX} for the *PhaseSep* case reduced to 4.454*10^{-5} from 1.479*10^{-4} for *NonPhaseSep* simulation. For southeastern United States, it is clear that an overall shift of higher γ_{IEPOX} values > 10^{-3} to lower values ranging between 10^{-4} to 10^{-6} occurs with introduction of phase separation and phase state parameters in CMAQ (Fig. S2). For continental United States, there is a similar trend with the shift in highest peak of the probability distribution of γ_{IEPOX} with *PhaseSep* case relative to *NonPhaseSep* case (Fig. 7A).

Figures 7B and 7C show the mean value of γ_{IEPOX} for each grid cell across the continental United States during the *PhaseSep* and *NonPhaseSep* simulations, respectively, for the 2013 SOAS period. The plot shows an overall reduction in γ_{IEPOX} when phase separation was introduced. There was high variability in the value of γ_{IEPOX} between regions; specifically, between the eastern and western United States. To understand the drivers that influence changes in γ_{IEPOX} with the new *PhaseSep* simulation, grid cells that exhibited the maximum increase and decrease relative to the *NonPhaseSep* were analyzed. When phase separation was included, particles in grid cell and time-step with maximum reduction in γ_{IEPOX} were the result of a low $D_{org,eff}$ of 5.83*10^{-19} m^2/s and an l_{org} as high as 100 nm resulting in a relatively thick organic coating with diffusion limitations. Particles in the grid cell and time-step with the highest increases in γ_{IEPOX} had a $D_{org,eff}$ value of

$7.34*10^{-16}$ m^2/s and l_{org} of 0.668 nm, and were located over oceans with an abundant amount of aerosol liquid water that were in close proximity to biogenic isoprene emission sources (Fig. S3). These large increases in γ_{IEPOX} were primarily caused by increases in $k_{particle}$ due to added nucleophiles (i.e. abundant aerosol liquid water) and a lack of diffusive limitations through the organic shell. Mean γ_{IEPOX} for the 2013 SOAS period across the continental United States shows a higher reduction in the *PhaseSep* (Fig. 7B) relative to *NonPhaseSep* (Fig. 7C), in regions such as the southwest US and southern Canada, with higher l_{org} (Fig. S3). To summarize, phase (which influences $D_{org,eff}$) and thickness (l_{org}) of the organic coating are the main drivers of change in γ_{IEPOX}. A recent study by Riva et al. (2019) demonstrated that the formation of organosulfates during the IEPOX reactive uptake process leads to an organic coating, and thus, a reduced γ_{IEPOX}. This manifests as a self-limiting effect during the IEPOX-derived SOA formation. Atmospheric models, including this work, do not consider this recently observed self-limiting process yet, but accounting for it may lead to a further reduction of the γ_{IEPOX}.

3.2.2 Predicted SOA mass

Variability in the values of γ_{IEPOX}, as calculated in the *PhaseSep* simulation (Fig. 7B) relative to the *NonPhaseSep* simulation (Fig. 7C), were also reflected in the large geospatial variations in the concentrations of IEPOX-derived SOA (i.e., organosulfates and tetrols (Fig. 8A)). Higher reduction in the IEPOX-derived SOA for *PhaseSep* relative to *NonPhaseSep* were also in regions such as the southwest United States and southern Canada (more pronounced near the Great Lakes), with higher reductions to γ_{IEPOX} owing to thick organic coatings (Fig. S3). Figure 8B shows the average relative change in predicted biogenic SOA mass. Although, the southwest United States shows high reduction in IEPOX-derived SOA (Fig. 8A), it is not reflected for changes in biogenic

SOA (Fig. 8B). While the high reduction in IEPOX-derived SOA (Fig. 8A) in southern Canada is reflected in reductions in biogenic SOA in that region (Fig. 8B). This spatial variability can be explained by the lower fraction of IEPOX-derived SOA in total biogenic SOA on average in southwest United States compared to their higher fraction in southern Canada near Great Lakes (Fig. S4A), which are further reduced to be negligible in the southwest US in the *PhaseSep* case (Fig. S4B). Hence, magnitude of changes in biogenic SOA (Fig. 8B) and eventually $PM_{2.5}$ organic carbon mass (Fig. S5) are dampened as compared to changes in IEPOX-derived SOA mass with introduction of phase separation parameters (Fig. 8A). On average, the largest reduction in biogenic SOA mass at any one grid cell was 40.9% and occurred over forested region in Ontario, Canada near Lake Superior (Fig. 8B) which also exhibits high IEPOX-derived SOA contribution to total biogenic SOA (Fig. S4). For southeastern United States, modeled average reductions for 2013 SOAS period in IEPOX-derived SOA ranged between 25-30%, which translated to 10-15% reduction in total biogenic SOA (Fig. 8). Whereas, the highest average reduction in IEPOX-derived SOA was 74.06% that occurred over Colorado (Fig. 8A), which eventually matters less in terms of overall biogenic SOA reduction (Fig. 8B) owing to negligible contribution of IEPOX-derived SOA to total biogenic SOA in the American southwest (Fig. S4). In the southern Canadian region near the Great Lakes where the maximum biogenic SOA reduction in *PhaseSep* occurred, the average reductions in IEPOX-derived SOA ranged from 63% to 66%. The southern Canadian region with maximum biogenic SOA reduction had average particle viscosities in the range of $1.3*10^3$ to $8.36*10^5$ Pa•s. The phase separation frequency of particles for southern Canada region was 86.3% of all time steps and was SSPS 62.04% of the time and LLPS 24.26% of the time. The combination of these factors led to a 52.64% average reduction in γ_{IEPOX}.

3.2.2.1 Comparison to Observed Data

Figure 9 shows that consideration of phase state and separation in CMAQ slightly worsened the NMB based on comparison with hourly $PM_{2.5}$ organic carbon mass SEARCH observations at both the Centreville rural site and Jefferson street, Atlanta urban site by ~ -4%. However, this change was marginal in terms of mean bias change in *PhaseSep* relative to *NonPhaseSep* case being < 0.1 μg/m^3. The sensitivity cases that assumed a higher H_{org} (*HighHorg*) and considered LLPS in predicting SSPS (*PhaseSep2*) resulted in correcting the worsening of model performance observed with *PhaseSep* case (Figs. 9 and S6). This highlights the importance of poorly constrained parameters in models like H_{org} assumed as a constant and factors that might govern phase separation under low RH or low aerosol water at different O:C ratios.

3.3 Sensitivities

The reduction in emission sources of NO_x and SO_2 impacted aerosol composition, and thus, the T_{org}. The average T_{org} for the emissions reduction simulation predicted a statistically significant (p-value = $2*10^{-16}$) increase of 1.5 K from the *PhaseSep* simulation, indicating the future emission reductions could result in an increase in viscosity and frequency of phase separation. The overall phase separation frequency for this sensitivity was 70.5% (57.0% SSPS, 13.5% LLPS) with predicted viscosities ranging from $6.13*10^{-3}$ to $1.73*10^{11}$ Pa•s, which was narrower as compared to η_{org} range from *PhaseSep* simulation (refer to section 3.1.1). With the implementation of the future NO_x and SO_2 emissions reductions, overall there was a mean 7.85% reduction in biogenic SOA at the surface level from the *PhaseSep* simulation for Continental United States. As shown in Figure 10A the areas with the largest reductions in SOA mass occurred in American southeast, while a marginal increase in SOA mass that occurred over the Atlantic Ocean and in some sparse areas in Northern Canada and Western United States. The American southeast was highly sensitive to the Emissions Reductions sensitivity due to the high concentrations of SO_2 from coal-fired power plants and the high concentrations of IEPOX-derived SOA, whose chemistry is driven by particulate sulfate. Fig. S7 shows that highest reductions in particulate sulfate occurs in the American southeast, which would be accompanied by the reduction in aerosol liquid water, driving the reductions in IEPOX-derived SOA as shown in recent literature (Pye et al., 2017), and hence the large reductions in biogenic SOA mass. Also, NO_x reductions in the NO_x-limited southeastern United States region essentially results in stronger decrease in biogenic SOA as shown by Fig. 10A, which is consistent with findings from SENEX aircraft (Edwards et al., 2017) and SOAS ground measurements (Xu et al., 2015) in the southeastern United States.

When increases in H_{org} were simulated in scenario *HighHorg* it had impacts in opposite directions compared to changes in the emission reduction scenario. This increase in biogenic SOA can simply be attributed to the increased dissolution of IEPOX into the particle phase through the organic coating with a three order of magnitude higher H_{org} relative to that in *PhaseSep* simulation. The average T_{org} in the *HighHorg* simulation had a statistically significant increase of 1.4 K, with particles being phase separated 68.3% of the time (55.8% SSPS, 12.5% LLPS). Predicted viscosities in this simulation ranged from $5.94*10^{-3}$ Pa•s to 6.10^{11} Pa•s. Overall, biogenic SOA mass increased by an average of 14.19% at the surface level for this simulation relative to *PhaseSep* for the Continental United States. As shown in Figure 10B, the regions with the largest increases in biogenic SOA mass were located over boreal forests in Ontario and Quebec, Canada that correspond to the regions with highest reactive uptake (Figs. 7B and 7C) forming more homogenous SOA with increased H_{org}.

The removal of the assumption that all particles with a semisolid viscosity were phase separated (*PhaseSep2*) decreased the overall phase separation frequency to 29.0% from 68.5% in the *PhaseSep* simulation. The entirety of this reduction was from reductions in SSPS. Figure 10C gives the changes in biogenic SOA mass yields in the *PhaseSep2* case relative to the *PhaseSep* case, with largest increases in Canadian regions where SSPS regime is moving to either LLPS or homogenous liquid mixture. This causes SOA yield increases explained by high reactive uptake in these regions (Figs. 7B and 7C). The phase separation frequency at the Centreville, Alabama site decreased to 65.4% from 79.3%. The average T_{org} increased by 2.3 K with a range of 137 K to 289 K and predicted viscosities ranged from $5.93*10^{-3}$ Pa•s- $9.99*10^{11}$ Pa•s. Overall biogenic SOA mass yields increased by an average of 25.86% from the *PhaseSep* simulation for Continental United States. The initial assumption regarding phase separation at high viscosity seems to be similarly as important as the assumption regarding H_{org} in constraining the impact of phase state and morphology on reactive uptake of IEPOX.

4 Discussion and Atmospheric Implications

Current chemical transport models have not accurately accounted for the effects of aerosol composition on phase separation or viscosity. This work has updated the CMAQ model to include parameters to calculate the T_{org} based on the Gordon-Taylor equation for SOA. This implementation used molar mass and O:C ratio of the species, but other parameters could be used. For example, DeRieux et al., (2018) developed a calculation for $T_{g,i}$ based on the number of carbon-hydrogen and carbon-oxygen bonds in a molecule. DeRieux et al., (2018) showed their implementation to be in good agreement with implementation provided in this work (Eq. (4)) for species with molar masses in the range of those used by CMAQv5.2.1. This implementation also included parameters to determine whether SOA was phase-separated based on its viscosity, O:C ratio, sulfate concentrations, and the ambient RH. Our model predicted that 68.5% of the time particles would exhibit phase separation at the surface layer, which is in proximity with the 70% predicted by Pye et al. (2017). This implementation predicts that most of the SOA in the middle and upper troposphere over the United States is phase separated with organics increasingly in a semi-solid or even glassy state with increasing altitude. This is in agreement with previous fieldwork and modeling studies which has found that SOA in the upper troposphere tends to be in a glassy state (Lienhard et al., 2015; Shiraiwa et al., 2017). This work also shows LLPS to be more dominant in the eastern US, while semi-solid phase state being more prevalent in western US. This is in agreement with the predominant role of aerosol liquid water driving the liquid phase state and LLPS across the eastern United States, as observed in previous studies (Pye et al., 2017, 2018).

The model predicted that SOA dominated by anthropogenic constituents typically featured thick semi-solid organic phases surrounding aqueous cores, which caused the reactive uptake of IEPOX to become diffusion limited. Regions that were predicted to have larger fractions of biogenic SOA mass typically featured LLPS morphology that did not produce much of diffusion limitations. These aerosols also resulted in a smaller inorganic core volume increasing the concentrations of nucleophiles and acids, thus enhancing the rate of reaction in presence of abundant aerosol water over oceans, but exhibited reduction in SOA over land though not as much as solid-like particles exhibited. The phase separation parameters had the largest impact over the Ohio River valley, southern Canada (more pronounced near Great Lakes) and American southeast. These areas were also the most sensitive to future emission reductions of NO_x and SO_2.

https://doi.org/10.5194/acp-2019-900
Preprint. Discussion started: 7 November 2019

Further experimental and modeling work is required to understand the effects of aerosol phase state on the viscosity of the inorganic core that cause variability in the value of D_a and can subsequently alter the reactive uptake of IEPOX. The conditions under which highly viscous SOA will separate from inorganics in a particle or if the particle will remain homogenously mixed should be further explored as well. Particle morphology in case of phase-separated organic and inorganic species as 'core-shell' or 'partially engulfed' or 'emulsified' (smaller islands of organics in the aqueous inorganic core) is driven by the differences in the interfacial surface tensions (Gorkowski et al., 2017). Recent studies have also shown that at very high RH ranges (95-100%), some particles will return to a core-shell morphology (Ham et al., 2019; Renbaum-Wolff et al., 2016). There is also little information on the criteria that drives this kind of phase separation as well. Such variability in particle morphologies may modify the value of $k_{particle}$ by changing the core volume. It is imperative that these parameters be better constrained in models. Furthermore, there is much uncertainty in the organic phase Henry's Law coefficient (H_{org}), where higher H_{org} increases the dissolution of IEPOX into the aerosol phase. Some of the newly proposed reaction mechanisms leading to the formation of extremely-low volatile organic compounds (ELVOCs) and organosulfates may also increase the viscosity of the particle phase, but have not been incorporated in this study.

This work paves the way for implementing a more accurate representation of multiphase chemistry of different complex systems on the lines of explicit representation of IEPOX SOA. Multiphase chemistry of other dominant SOA apart from IEPOX SOA, such as monoterpene-derived SOA, are not incorporated in CMAQv5.2.1 (Pye et al., 2018; Slade et al., 2019), and should be a focus of future work. This work showed that organic water fraction is the biggest driver of viscosity, though the water abundance was set at 10% of the inorganic water content. Organic water uptake, even if increased, will still follow the diurnal trend of RH since it is diverted from the aqueous core that is derived from ISORRORPIA-based aerosol water in CMAQ v5.2.1. It does not, however, consider the hydrophobicity or abundance of various organic constituents. Constraining abundance of organic water uptake in terms of its association with different organic species and evaluating its reduction with future emission reductions of SO_x (SO_2 and sulfate) will be pertinent for future work.

Performing sensitivity simulations over the *PhaseSep* parametrization as part of this work also show that any assumptions made on determining phase separation or morphology (*PhaseSep2*) is as important as constraining the H_{org} ($HighH_{org}$) factor in the regions with abundant IEPOX SOA such as, American and Canadian southeast. Incorporating explicit kinetics coupled with thermodynamic calculation of energies governing the mixing state of organic-inorganic aerosol mixtures under different aerosol phase states, as observed from recent and ongoing experimental findings, into atmospheric models such as CMAQ, would lead to more scientifically sound representations of the impact particle phase state and morphology have on SOA mass predictions.

Code availability

US EPA makes the source code of CMAQ version 5.2.1 model publicly available for download at: https://github.com/USEPA/CMAQ/tree/5.2.1 (last access: 6 November 2019). Corresponding author can make the modifications made to the CMAQ source code as part of this work available on request.

Data availability

The emissions and meteorological inputs along with other miscellaneous inputs to run CMAQ model for the SOAS 2013 episode (1 June 2013 to 15 July 2015) across continental United States can be downloaded from: https://drive.google.com/open?id=1XR6Xp3bZzrZIzNBx-AgjcNCtC_HLlCkZ, made available by US EPA and University of North Carolina-Institute of Environment (last access: 6 November 2019).

Author contributions

RS and QZR lead the writing with WV. RS designed the new *PhaseSep* methodology along with sensitivity cases to run in consistent consultation with YZ, HOTP, YC, JDS, QZR and WV. QZR implemented the model code and performed the simulations in the regional scale model with reviews from HOTP. RS analyzed results of simulations with QZR, WV and HZ. BHL, CM, FDL-H, JAT, AHG and HZ analyzed the SOAS field data. RS and QZR prepared the paper with extensive reviews and edits from WV, YZ, YC, HOTP, HZ, and JDS.

Competing interests

The authors declare that they have no conflict of interest.

Disclaimer: The U.S. Environmental Protection Agency through its Office of Research and Development collaborated in the research described here. The research has been subjected to Agency administrative review and approved for publication but may not necessarily reflect official Agency policy. The views expressed in this article are those of the authors and do not necessarily represent the views or policies of the U.S. Environmental Protection Agency.

Acknowledgements

A National Science Foundation (NSF) Postdoctoral Fellowship under Atmospheric and Geospace Sciences (AGS-1524731) and the National Institute of Health (NIH) training grant supported YZ. HZ and AHG were supported by NSF Grants AGS-1250569 and AGS-1644406. BHL, FDL, CM, and JAT were supported by a grant from the U.S. Department of Energy Atmospheric System Research Program (DE-SC0018221). JDS, YC, and YZ were supported by NSF-AGS grant 1703535.

References

Eyth, A., Zubrow, A., and Mason, R: Technical Support Document (TSD): Preparation of Emissions Inventories for the Version 6.1, 2011 Emissions Modeling Platform, [online] Available from: http://www.epa.gov/ttn/chief/emch/2011v6/2011v6.1_2018_2025_base_EmisMod_TSD_nov2014_v6.pdf (Accessed 20 November 2018), 2014.

Anttila, T., Kiendler-Scharr, A., Tillmann, R. and Mentel, T. F.: On the Reactive Uptake of Gaseous Compounds by Organic-Coated Aqueous Aerosols: Theoretical Analysis and Application to the Heterogeneous Hydrolysis of N2O5, J. Phys. Chem. A, 110(35), 10435–10443, doi:10.1021/jp062403c, 2006.

Appel, K. W., Napelenok, S. L., Foley, K. M., Pye, H. O. T., Hogrefe, C., Luecken, D. J., Bash, J. O., Roselle, S. J., Pleim, J. E., Foroutan, H., Hutzell, W. T., Pouliot, G. A., Sarwar, G., Fahey, K. M., Gantt, B., Gilliam, R. C., Heath, N. K., Kang, D., Mathur, R., Schwede, D. B., Spero, T. L., Wong, D. C. and Young, J. O.: Description and evaluation of the Community Multiscale Air Quality (CMAQ) modeling system version 5.1, Geosci Model Dev, 10(4), 1703–1732, doi:10.5194/gmd-10-1703-2017, 2017.

Bash, J. O., Baker, K. R. and Beaver, M. R.: Evaluation of improved land use and canopy representation in BEIS v3.61 with biogenic VOC measurements in California, Geoscientific Model Development, 9(6), 2191–2207, doi:https://doi.org/10.5194/gmd-9-2191-2016, 2016.

Bates, K. H., Crounse, J. D., St. Clair, J. M., Bennett, N. B., Nguyen, T. B., Seinfeld, J. H., Stoltz, B. M. and Wennberg, P. O.: Gas Phase Production and Loss of Isoprene Epoxydiols, J. Phys. Chem. A, 118(7), 1237–1246, doi:10.1021/jp4107958, 2014.

Bateman, A. P., Bertram, A. K., and Martin, S. T.: Hygroscopic Influence on the Semisolid-to-Liquid Transition of Secondary Organic Materials, The Journal of Physical Chemistry A, 119, 4386-4395, 10.1021/jp508521c, 2015a.

Bateman, A. P., Gong, Z., Liu, P., Sato, B., Cirino, G., Zhang, Y., Artaxo, P., Bertram, A. K., Manzi, A. O., Rizzo, L. V., Souza, R. A. F., Zaveri, R. A., and Martin, S. T.: Sub-micrometre particulate matter is primarily in liquid form over Amazon rainforest, Nature Geoscience, 9, 34, 10.1038/ngeo2599 https://www.nature.com/articles/ngeo2599#supplementary-information, 2015b.

Bateman, A. P., Gong, Z., Harder, T. H., de Sá, S. S., Wang, B., Castillo, P., China, S., Liu, Y., O'Brien, R. E., Palm, B. B., Shiu, H. W., Cirino, G. G., Thalman, R., Adachi, K., Alexander, M. L., Artaxo, P., Bertram, A. K., Buseck, P. R., Gilles, M. K., Jimenez, J. L., Laskin, A., Manzi, A. O., Sedlacek, A., Souza, R. A. F., Wang, J., Zaveri, R., and Martin, S. T.: Anthropogenic influences on the physical state of submicron particulate matter over a tropical forest, Atmos. Chem. Phys., 17, 1759-1773, 10.5194/acp-17-1759-2017, 2017.

Bertram, A. K., Martin, S. T., Hanna, S. J., Smith, M. L., Bodsworth, A., Chen, Q., Kuwata, M., Liu, A., You, Y., and Zorn, S. R.: Predicting the relative humidities of liquid-liquid phase separation, efflorescence, and deliquescence of mixed particles of ammonium sulfate, organic material, and water using the organic-to-sulfate mass ratio of the particle and the oxygen-to-carbon elemental ratio of the organic component, Atmos. Chem. Phys., 11, 10995-11006, 10.5194/acp-11-10995-2011, 2011.

Bondy, A. L., Craig, R. L., Zhang, Z., Gold, A., Surratt, J. D. and Ault, A. P.: Isoprene-Derived Organosulfates: Vibrational Mode Analysis by Raman Spectroscopy, Acidity-Dependent Spectral Modes, and Observation in Individual Atmospheric Particles, J Phys Chem A, 122(1), 303–315, doi:10.1021/acs.jpca.7b10587, 2018.

Budisulistiorini, S. H., Baumann, K., Edgerton, E. S., Bairai, S. T., Mueller, S., Shaw, S. L., Knipping, E. M., Gold, A. and Surratt, J. D.: Seasonal characterization of submicron aerosol chemical composition and organic aerosol sources in the southeastern United States: Atlanta, Georgia,and Look Rock, Tennessee, Atmospheric Chemistry and Physics, 16(8), 5171–5189, doi:https://doi.org/10.5194/acp-16-5171-2016, 2016.

Budisulistiorini, S. H., Nenes, A., Carlton, A. G., Surratt, J. D., McNeill, V. F. and Pye, H. O. T.: Simulating Aqueous-Phase Isoprene-Epoxydiol (IEPOX) Secondary Organic Aerosol Production During the 2013 Southern Oxidant and Aerosol Study (SOAS), Environ. Sci. Technol., 51(9), 5026–5034, doi:10.1021/acs.est.6b05750, 2017.

Carlton, A. G. and Baker, K. R.: Photochemical Modeling of the Ozark Isoprene Volcano: MEGAN, BEIS, and Their Impacts on Air Quality Predictions, Environ. Sci. Technol., 45(10), 4438–4445, doi:10.1021/es200050x, 2011.

Carslaw, K. S., Lee, L. A., Reddington, C. L., Pringle, K. J., Rap, A., Forster, P. M., Mann, G. W., Spracklen, D. V., Woodhouse, M. T., Regayre, L. A. and Pierce, J. R.: Large contribution of natural aerosols to uncertainty in indirect forcing, Nature, 503(7474), 67–71, doi:10.1038/nature12674, 2013.

Chenyakin, Y.: Are diffusion coefficients calculated using the Stokes-Einstein equation combined with viscosities consistent with measured diffusion coefficients of tracer organics within organics-water mediums?, University of British Columbia., 2015.

Cui, T., Zeng, Z., dos Santos, E. O., Zhang, Z., Chen, Y., Zhang, Y., Rose, C. A., Budisulistiorini, S. H., Collins, L. B., Bodnar, W. M., de Souza, R. A. F., Martin, S. T., Machado, C. M. D., Turpin, B. J., Gold, A., Ault, A. P., and Surratt, J. D.: Development of a hydrophilic interaction liquid chromatography (HILIC) method for the chemical characterization of water-soluble isoprene epoxydiol (IEPOX)-derived secondary organic aerosol, Environmental Science: Processes & Impacts, 20, 1524-1536, 10.1039/C8EM00308D, 2018.

DeRieux, W.-S. W., Li, Y., Lin, P., Laskin, J., Laskin, A., Bertram, A. K., Nizkorodov, S. A. and Shiraiwa, M.: Predicting the glass transition temperature and viscosity of secondary organic material using molecular composition, Atmospheric Chemistry and Physics, 18(9), 6331–6351, doi:https://doi.org/10.5194/acp-18-6331-2018, 2018.

Docherty, K. S., Stone, E. A., Ulbrich, I. M., DeCarlo, P. F., Snyder, D. C., Schauer, J. J., Peltier, R. E., Weber, R. J., Murphy, S. M., Seinfeld, J. H., Grover, B. D., Eatough, D. J. and Jimenez, J. L.: Apportionment of primary and secondary organic aerosols in southern California during the 2005 study of organic aerosols in riverside (SOAR-1), Environ. Sci. Technol., 42(20), 7655–7662, 2008.

Eddingsaas, N. C., VanderVelde, D. G., and Wennberg, P. O.: Kinetics and products of the acid-catalyzed ring-opening of atmospherically relevant butyl epoxy alcohols, The Journal of Physical Chemistry A, 114, 8106-8113, DOI: 10.1021/jp103907c, 2010.

Edwards, P. M., Aikin, K. C., Dube, W. P., Fry, J. L., Gilman, J. B., de Gouw, J. A., Graus, M. G., Hanisco, T. F., Holloway, J., Hübler, G., Kaiser, J., Keutsch, F. N., Lerner, B. M., Neuman, J. A., Parrish, D. D., Peischl, J., Pollack, I. B., Ravishankara, A. R., Roberts, J. M., Ryerson, T. B., Trainer, M., Veres, P. R., Wolfe, G. M., Warneke, C., and Brown, S. S.: Transition from high- to low-NOx control of night-time oxidation in the southeastern US, Nature Geoscience, 10, 490, 10.1038/ngeo2976, https://www.nature.com/articles/ngeo2976#supplementary-information, 2017.

Emery, C., Jung, J., Koo, B. and Yarwood, G.: Improvements to CAMx Snow Cover Treatments and Carbon Bond Chemical Mechanism for Winter Ozone. Final report for Utah DAQ, Utah Department of Air Quality., 2015.

Evoy, E., Maclean, A. M., Rovelli, G., Li, Y., Tsimpidi, A. P., Karydis, V. A., Kamal, S., Lelieveld, J., Shiraiwa, M., Reid, J. P., and Bertram, A. K.: Predictions of diffusion rates of large organic molecules in secondary organic aerosols using the Stokes–Einstein and fractional Stokes–Einstein relations, Atmos. Chem. Phys., 19, 10073-10085, 10.5194/acp-19-10073-2019, 2019.

Freedman, M. A.: Phase separation in organic aerosol, Chem. Soc. Rev., 46(24), 7694–7705, doi:10.1039/C6CS00783J, 2017.

Fulcher, G. S.: Analysis of recent measurements of viscosity of glasses, J. Amer. Ceram. Soc, 8, 339–355, 1925.

Gaston, C. J., Riedel, T. P., Zhang, Z., Gold, A., Surratt, J. D. and Thornton, J. A.: Reactive Uptake of an Isoprene-Derived Epoxydiol to Submicron Aerosol Particles, Environmental Science & Technology, 48(19), 11178–11186, doi:10.1021/es5034266, 2014.

Gordon, M. and Taylor, J.: Ideal Copolymers and the Second-Order Transitions of Synthetic Rubbers. I. Non-Crystalline Copolymers, Journal of Applied Chemistry, 2(9), 493–500, doi:10.1002/jctb.5010020901, 1952.

Gorkowski, K., Donahue, N. M. and Sullivan, R. C.: Emulsified and liquid–liquid phase-separated states of α-pinene secondary organic aerosol determined using aerosol optical tweezers, Environmental Science & technology, 51(21), 12154-12163, doi:10.1021/acs.est.7b03250, 2017.

Grandey, B. S., Rothenberg, D., Avramov, A., Jin, Q., Lee, H.-H., Liu, X., Lu, Z., Albani, S. and Wang, C.: Effective radiative forcing in the aerosol–climate model CAM5.3-MARC-ARG, Atmospheric Chemistry and Physics, 18(21), 15783–15810, doi:10.5194/acp-18-15783-2018, 2018.

Grayson, J. W., Zhang, Y., Mutzel, A., Renbaum-Wolff, L., Böge, O., Kamal, S., Herrmann, H., Martin, S. T. and Bertram, A. K.: Effect of varying experimental conditions on the viscosity of <i>α</i>-pinene derived secondary organic material, Atmospheric Chemistry and Physics, 16(10), 6027–6040, doi:10.5194/acp-16-6027-2016, 2016.

Grayson, J. W., Evoy, E., Song, M., Chu, Y., Maclean, A., Nguyen, A., Upshur, M. A., Ebrahimi, M., Chan, C. K., Geiger, F. M., Thomson, R. J. and Bertram, A. K.: The effect of hydroxyl functional groups and molar mass on the viscosity of non-crystalline organic and organic-water particles, Atmospheric Chemistry and Physics, 17(13), 8509–8524, doi:10.5194/acp-17-8509-2017, 2017.

Guenther, A., Karl, T., Harley, P., Wiedinmyer, C., Palmer, P. I. and Geron, C.: Estimates of global terrestrial isoprene emissions using MEGAN (Model of Emissions of Gases and Aerosols from Nature), Atmospheric Chemistry and Physics, 6(11), 3181–3210, doi:https://doi.org/10.5194/acp-6-3181-2006, 2006.

Ham, S., Babar, Z. B., Lee, J., Lim, H. and Song, M.: Liquid-liquid phase separation in secondary organic aerosol particles produced from α-pinene ozonolysis and α-pinene photo-oxidation with/without ammonia, Atmos. Chem. Phys. Discuss., 1–27, doi:10.5194/acp-2019-19, 2019.

Hansen, D. A., Edgerton, E. S., Hartsell, B. E., Jansen, J. J., Kandasamy, N., Hidy, G. M. and Blanchard, C. L.: The Southeastern Aerosol Research and Characterization Study: Part 1—Overview, Journal of the Air & Waste Management Association, 53(12), 1460–1471, doi:10.1080/10473289.2003.10466318, 2003.

Heath, N. K., Pleim, J. E., Gilliam, R. C. and Kang, D.: A simple lightning assimilation technique for improving retrospective WRF simulations, Journal of Advances in Modeling Earth Systems, 8(4), 1806–1824, doi:10.1002/2016MS000735, 2016.

Hildebrant Ruiz, L. and Yarwood, G.: Interactions between Organic Aerosol and NOy: Influence on Oxidant Production., University of Texas at Austin. [online] Available from: http://aqrp.ceer.utexas.edu/projectinfoFY12_13/12-012/12-012%20Final%20Report.pdf, 2013.

Huang, W., Saathoff, H., Pajunoja, A., Shen, X., Naumann, K.-H., Wagner, R., Virtanen, A., Leisner, T. and Mohr, C.: α-Pinene secondary organic aerosol at low temperature: chemical composition and implications for particle viscosity, Atmospheric Chemistry and Physics, 18(4), 2883–2898, doi:https://doi.org/10.5194/acp-18-2883-2018, 2018.

Hwang, S.-H., Lee, J. Y., Yi, S.-M. and Kim, H.: Associations of particulate matter and its components with emergency room visits for cardiovascular and respiratory diseases, PLOS ONE, 12(8), e0183224, doi:10.1371/journal.pone.0183224, 2017.

Jacobs, M. I., Burke, W. J. and Elrod, M. J.: Kinetics of the reactions of isoprene-derived hydroxynitrates: gas phase epoxide formation and solution phase hydrolysis, Atmospheric Chemistry and Physics, 14(17), 8933–8946, doi:https://doi.org/10.5194/acp-14-8933-2014, 2014.

Jaques, P. A. and Kim, C. S.: Measurement of total lung deposition of inhaled ultrafine particles in healthy men and women, Inhal Toxicol, 12(8), 715–731, doi:10.1080/08958370050085156, 2000.

Koop, T., Bookhold, J., Shiraiwa, M. and Pöschl, U.: Glass transition and phase state of organic compounds: dependency on molecular properties and implications for secondary organic aerosols in the atmosphere, Phys. Chem. Chem. Phys., 13(43), 19238–19255, doi:10.1039/C1CP22617G, 2011.

Krechmer, J. E., Coggon, M. M., Massoli, P., Nguyen, T. B., Crounse, J. D., Hu, W., Day, D. A., Tyndall, G. S., Henze, D. K., Rivera-Rios, J. C., Nowak, J. B., Kimmel, J. R., Mauldin, R. L., Stark, H., Jayne, J. T., Sipilä, M., Junninen, H., Clair, J. M. S., Zhang, X., Feiner, P. A., Zhang, L., Miller, D. O., Brune, W. H., Keutsch, F. N., Wennberg, P. O., Seinfeld, J. H., Worsnop, D. R., Jimenez, J. L. and Canagaratna, M. R.: Formation of Low Volatility Organic Compounds and Secondary Organic Aerosol from Isoprene Hydroxyhydroperoxide Low-NO Oxidation, Environ. Sci. Technol., 49(17), 10330–10339, doi:10.1021/acs.est.5b02031, 2015.

Lee, L. A., Reddington, C. L. and Carslaw, K. S.: On the relationship between aerosol model uncertainty and radiative forcing uncertainty, PNAS, 113(21), 5820–5827, doi:10.1073/pnas.1507050113, 2016.

Liao, J., Froyd, K. D., Murphy, D. M., Keutsch, F. N., Yu, G., Wennberg, P. O., St Clair, J. M., Crounse, J. D., Wisthaler, A., Mikoviny, T., Jimenez, J. L., Campuzano-Jost, P., Day, D. A., Hu, W., Ryerson, T. B., Pollack, I. B., Peischl, J., Anderson, B. E., Ziemba, L. D., Blake, D. R., Meinardi, S. and Diskin, G.: Airborne measurements of organosulfates over the continental U.S, J Geophys Res Atmos, 120(7), 2990–3005, doi:10.1002/2014JD022378, 2015.

Lienhard, D. M., Huisman, A. J., Krieger, U. K., Rudich, Y., Marcolli, C., Luo, B. P., Bones, D. L., Reid, J. P., Lambe, A. T., Canagaratna, M. R., Davidovits, P., Onasch, T. B., Worsnop, D. R., Steimer, S. S., Koop, T. and Peter, T.: Viscous organic aerosol particles in the upper troposphere: diffusivity-controlled water uptake and ice nucleation?, Atmospheric Chemistry and Physics, 15(23), 13599–13613, doi:https://doi.org/10.5194/acp-15-13599-2015, 2015.

Lopez-Hilfiker, F. D., Mohr, C., D'Ambro, E. L., Lutz, A., Riedel, T. P., Gaston, C. J., Iyer, S., Zhang, Z., Gold, A., Surratt, J. D., Lee, B. H., Kurten, T., Hu, W. W., Jimenez, J., Hallquist, M., and Thornton, J. A.: Molecular Composition and Volatility of Organic Aerosol in the Southeastern U.S.: Implications for IEPOX Derived SOA, Environmental Science & Technology, 50, 2200-2209, 10.1021/acs.est.5b04769, 2016.

Maclean, A. M., Butenhoff, C. L., Grayson, J. W., Barsanti, K., Jimenez, J. L. and Bertram, A. K.: Mixing times of organic molecules within secondary organic aerosol particles: a global planetary boundary layer perspective, Atmospheric Chemistry and Physics, 17(21), 13037–13048, doi:10.5194/acp-17-13037-2017, 2017.

Marais, E. A., Jacob, D. J., Jimenez, J. L., Campuzano-Jost, P., Day, D. A., Hu, W., Krechmer, J., Zhu, L., Kim, P. S., Miller, C. C., Fisher, J. A., Travis, K., Yu, K., Hanisco, T. F., Wolfe, G. M., Arkinson, H. L., Pye, H. O. T., Froyd, K. D., Liao, J. and McNeill, V. F.: Aqueous-phase mechanism for secondary organic aerosol formation from isoprene: application to the southeast United States and co-benefit of SO_2 emission controls, Atmospheric Chemistry and Physics, 16(3), 1603–1618, doi:https://doi.org/10.5194/acp-16-1603-2016, 2016.

Marcolli, C., Luo, B. and Peter, T.: Mixing of the Organic Aerosol Fractions: Liquids as the Thermodynamically Stable Phases, J. Phys. Chem. A, 108(12), 2216–2224, doi:10.1021/jp036080l, 2004.

Marsh, A., Petters, S. S., Rothfuss, N. E., Rovelli, G., Song, Y. C., Reid, J. P. and Petters, M. D.: Amorphous phase state diagrams and viscosity of ternary aqueous organic/organic and inorganic/organic mixtures, Physical Chemistry Chemical Physics, 20, 15086–15097, doi:10.1039/c8cp00760h, 2018.

Martin, S. T.: Phase Transitions of Aqueous Atmospheric Particles, Chem. Rev., 100(9), 3403–3454, doi:10.1021/cr990034t, 2000.

Murphy, B. N., Woody, M. C., Jimenez, J. L., Carlton, A. M. G., Hayes, P. L., Liu, S., Ng, N. L., Russell, L. M., Setyan, A., Xu, L., Young, J., Zaveri, R. A., Zhang, Q., and Pye, H. O. T.: Semivolatile POA and parameterized total combustion SOA in CMAQv5.2: impacts on source strength and partitioning, Atmos. Chem. Phys., 17, 11107-11133, 10.5194/acp-17-11107-2017, 2017.

Nozière, B., Kalberer, M., Claeys, M., Allan, J., D'Anna, B., Decesari, S., Finessi, E., Glasius, M., Grgić, I., Hamilton, J. F., Hoffmann, T., Iinuma, Y., Jaoui, M., Kahnt, A., Kampf, C. J., Kourtchev, I., Maenhaut, W., Marsden, N., Saarikoski, S., Schnelle-Kreis, J., Surratt, J. D., Szidat, S., Szmigielski, R. and Wisthaler, A.: The molecular identification of organic compounds in the atmosphere: state of the art and challenges, Chem. Rev., 115(10), 3919–3983, doi:10.1021/cr5003485, 2015.

O'Brien, R. E., Wang, B., Kelly, S. T., Lundt, N., You, Y., Bertram, A. K., Leone, S. R., Laskin, A. and Gilles, M. K.: Liquid-liquid phase separation in aerosol particles: imaging at the nanometer scale, Environ. Sci. Technol., 49(8), 4995–5002, doi:10.1021/acs.est.5b00062, 2015.

Pajunoja, A., Malila, J., Hao, L., Joutsensaari, J., Lehtinen, K. E. J. and Virtanen, A.: Estimating the Viscosity Range of SOA Particles Based on Their Coalescence Time, Aerosol Science and Technology, 48(2), i–iv, doi:10.1080/02786826.2013.870325, 2014.

Paulot, F., Crounse, J. D., Kjaergaard, H. G., Kürten, A., St Clair, J. M., Seinfeld, J. H. and Wennberg, P. O.: Unexpected epoxide formation in the gas-phase photooxidation of isoprene, Science, 325(5941), 730–733, doi:10.1126/science.1172910, 2009.

Price, H. C., Mattsson, J., Zhang, Y., Bertram, A. K., Davies, J. F., Grayson, J. W., Martin, S. T., O'Sullivan, D., Reid, J. P., Rickards, A. M. J. and Murray, B. J.: Water diffusion in atmospherically relevant α-pinene secondary organic material †Electronic supplementary information (ESI) available. See DOI: 10.1039/c5sc00685f Click here for additional data file., Chem Sci, 6(8), 4876–4883, doi:10.1039/c5sc00685f, 2015.

Pye, H. O. T., Pinder, R. W., Piletic, I. R., Xie, Y., Capps, S. L., Lin, Y. H., Surratt, J. D., Zhang, Z., Gold, A., Luecken, D. J., Hutzell, W. T., Jaoui, M., Offenberg, J. H., Kleindienst, T. E., Lewandowski, M. and Edney, E. O.: Epoxide pathways improve model predictions of isoprene markers and reveal key role of acidity in aerosol formation, E and T Contents, 47(19), 11056–11064, doi:10.1021/es402106h, 2013.

Pye, H. O. T., Murphy, B. N., Xu, L., Ng, N. L., Carlton, A. G., Guo, H., Weber, R., Vasilakos, P., Appel, K. W., Budisulistiorini, S. H., Surratt, J. D., Nenes, A., Hu, W., Jimenez, J. L., Isaacman-VanWertz, G., Misztal, P. K. and Goldstein, A. H.: On the implications of aerosol liquid water and phase separation for organic aerosol mass, Atmospheric Chemistry and Physics, 17(1), 343–369, doi:10.5194/acp-17-343-2017, 2017.

Pye, H. O. T., Zuend, A., Fry, J. L., Isaacman-VanWertz, G., Capps, S. L., Appel, K. W., Foroutan, H., Xu, L., Ng, N. L. and Goldstein, A. H.: Coupling of organic and inorganic aerosol systems and the effect on gas–particle partitioning in the southeastern US, Atmos Chem Phys, 18(1), 357–370, doi:10.5194/acp-18-357-2018, 2018.

Regayre, L. A., Pringle, K. J., Lee, L. A., Rap, A., Browse, J., Mann, G. W., Reddington, C. L., Carslaw, K. S., Booth, B. B. B. and Woodhouse, M. T.: The Climatic Importance of Uncertainties in Regional Aerosol–Cloud Radiative Forcings over Recent Decades, J. Climate, 28(17), 6589–6607, doi:10.1175/JCLI-D-15-0127.1, 2015.

Reid, J. P., Bertram, A. K., Topping, D. O., Laskin, A., Martin, S. T., Petters, M. D., Pope, F. D., and Rovelli, G.: The viscosity of atmospherically relevant organic particles, Nature Communications, 9, 956, 10.1038/s41467-018-03027-z, 2018.

Renbaum-Wolff, L., Grayson, J. W., Bateman, A. P., Kuwata, M., Sellier, M., Murray, B. J., Shilling, J. E., Martin, S. T., and Bertram, A. K.: Viscosity of α-pinene secondary organic material and implications for particle growth and reactivity, Proceedings of the National Academy of Sciences, 110, 8014-8019, 10.1073/pnas.1219548110, 2013.

Renbaum-Wolff, L., Song, M., Marcolli, C., Zhang, Y., Liu, P. F., Grayson, J. W., Geiger, F. M., Martin, S. T. and Bertram, A. K.: Observations and implications of liquid-liquid phase separation at high relative humidities in secondary organic material produced by α-pinene ozonolysis without inorganic salts, Atmospheric Chemistry and Physics, 16(12), 7969–7979, doi:10.5194/acp-16-7969-2016, 2016.

Riedel, T., Lin, Y.-H., Zhang, Z., Chu, K., Thornton, J., Vizuete, W., Gold, A., Surratt, J. D.: Constraining condensed-phase formation kinetics of secondary organic aerosol components from isoprene epoxydiols, Atmospheric Chemistry and Physics, 16, 1245-1254, 2016.

Riemer, N., Vogel, H., Vogel, B., Anttila, T., Kiendler-Scharr, A., and Mentel, T. F.: Relative importance of organic coatings for the heterogeneous hydrolysis of N2O5 during summer in Europe, J. Geophys. Res.-Atmos., 114, D17307, https://doi.org/10.1029/2008JD011369, 2009.

Riva, M., Chen, Y., Zhang, Y., Lei, Z., Olson, N. E., Boyer, H. C., Narayan, S., Yee, L. D., Green, H. S., Cui, T., Zhang, Z., Baumann, K., Fort, M., Edgerton, E., Budisulistiorini, S. H., Rose, C. A., Ribeiro, I. O., e Oliveira, R. L., dos Santos, E. O., Machado, C. M. D., Szopa, S., Zhao, Y., Alves, E. G., de Sá, S. S., Hu, W., Knipping, E. M., Shaw, S. L., Duvoisin Junior, S., de Souza, R. A. F., Palm, B. B., Jimenez, J.-L., Glasius, M., Goldstein, A. H., Pye, H. O. T., Gold, A., Turpin, B. J., Vizuete, W., Martin, S. T., Thornton, J. A., Dutcher, C. S., Ault, A. P., and Surratt, J. D.: Increasing Isoprene Epoxydiol-to-Inorganic Sulfate Aerosol Ratio Results in Extensive Conversion of Inorganic Sulfate to Organosulfur Forms: Implications for Aerosol Physicochemical Properties, Environmental Science & Technology, 53, 8682-8694, 10.1021/acs.est.9b01019, 2019.

Ryder, O. S., Ault, A. P., Cahill, J. F., Guasco, T. L., Riedel, T. P., Cuadra-Rodriguez, L. A., Gaston, C. J., Fitzgerald, E., Lee, C., Prather, K. A. and Bertram, T. H.: On the role of particle inorganic mixing state in the reactive uptake of N2O5 to ambient aerosol particles, Environ. Sci. Technol., 48(3), 1618–1627, doi:10.1021/es4042622, 2014.

Schmedding, R., Ma, M., Zhang, Y., Farrell, S., Pye, H. O. T., Chen, Y., Wang, C.-T., Rasool, Q. Z., Budisulistiorini, S., Ault, A. P., Surratt, J. and Vizuete, W.: α-Pinene-Derived organic coatings on acidic sulfate aerosol impacts secondary organic aerosol formation from isoprene in a box model, Atmos. Environ., 213, 456-462, https://doi.org/10.1016/j.atmosenv.2019.06.005, 2019.

Shiraiwa, M., Li, Y., Tsimpidi, A. P., Karydis, V. A., Berkemeier, T., Pandis, S. N., Lelieveld, J., Koop, T. and Pöschl, U.: Global distribution of particle phase state in atmospheric secondary organic aerosols, Nature Communications; London, 8, 15002, doi:http://dx.doi.org.libproxy.lib.unc.edu/10.1038/ncomms15002, 2017.

Slade, J. H., Ault, A. P., Bui, A., Ditto, J., Lei, Z., Bondy, A. L., Olson, N. E., Cook, R. D., Desrochers, S. J., Harvey, R.M., Erickson, M. H., Wallace, H. W., Alvarez, S. L., Flynn, J. H., Boor, B. E., Petrucci, G. A., Gentner, D. R., Griffin, R. J. and Shepson, P. B.: Bouncier particles at night: biogenic secondary organic aerosol chemistry and sulfate drive diel variations in the aerosol phase in a mixed forest, Environ. Sci. Technol., 53(9), 4977-4987, DOI: 10.1021/acs.est.8b07319, 2019.

https://doi.org/10.5194/acp-2019-900
Preprint. Discussion started: 7 November 2019

Song, M., Liu, P. F., Hanna, S. J., Li, Y. J., Martin, S. T. and Bertram, A. K.: Relative humidity-dependent viscosities of isoprene-derived secondary organic material and atmospheric implications for isoprene-dominant forests, Atmospheric Chemistry and Physics, 15(9), 5145–5159, doi:10.5194/acp-15-5145-2015, 2015.

Song, M., Liu, P. F., Hanna, S. J., Zaveri, R. A., Potter, K., You, Y., Martin, S. T. and Bertram, A. K.: Relative humidity-dependent viscosity of secondary organic material from toluene photo-oxidation and possible implications for organic particulate matter over megacities, Atmospheric Chemistry and Physics, 16(14), 8817–8830, doi:10.5194/acp-16-8817-2016, 2016.

Song, M., Ham, S., Andrews, R. J., You, Y. and Bertram, A. K.: Liquid–liquid phase separation in organic particles containing one and two organic species: importance of the average O&thinsp;:&thinsp;C, Atmospheric Chemistry and Physics, 18(16), 12075–12084, doi:10.5194/acp-18-12075-2018, 2018.

Surratt, J. D., Murphy, S. M., Kroll, J. H., Ng, N. L., Hildebrandt, L., Sorooshian, A., Szmigielski, R., Vermeylen, R., Maenhaut, W., Claeys, M., Flagan, R. C. and Seinfeld, J. H.: Chemical composition of secondary organic aerosol formed from the photooxidation of isoprene, J Phys Chem A, 110(31), 9665–9690, doi:10.1021/jp061734m, 2006.

Surratt, J. D., Lewandowski, M., Offenberg, J. H., Jaoui, M., Kleindienst, T. E., Edney, E. O. and Seinfeld, J. H.: Effect of Acidity on Secondary Organic Aerosol Formation from Isoprene, Environmental Science & Technology, 41(15), 5363–5369, doi:10.1021/es0704176, 2007.

Surratt, J. D., Chan, A. W. H., Eddingsaas, N. C., Chan, M., Loza, C. L., Kwan, A. J., Hersey, S. P., Flagan, R. C., Wennberg, P. O. and Seinfeld, J. H.: Reactive intermediates revealed in secondary organic aerosol formation from isoprene, Proceedings of the National Academy of Sciences, 107(15), 6640–6645, doi:10.1073/pnas.0911114107, 2010.

Tamman, G. and Hesse, W.: The dependence of viscosity upon the temperature of supercooled liquids., Z. Anorg. Allg. Chem, 156, 245–257, 1926.

Ullmann, D. A., Hinks, M. L., Maclean, A. M., Butenhoff, C. L., Grayson, J. W., Barsanti, K., Jimenez, J. L., Nizkorodov, S. A., Kamal, S., and Bertram, A. K.: Viscosities, diffusion coefficients, and mixing times of intrinsic fluorescent organic molecules in brown limonene secondary organic aerosol and tests of the Stokes–Einstein equation, Atmos. Chem. Phys., 19, 1491-1503, 10.5194/acp-19-1491-2019, 2019.

Virtanen, A., Joutsensaari, J., Koop, T., Kannosto, J., Yli-Pirilä, P., Leskinen, J., Mäkelä, J. M., Holopainen, J. K., Pöschl, U., Kulmala, M., Worsnop, D. R., and Laaksonen, A.: An amorphous solid state of biogenic secondary organic aerosol particles, Nature, 467, 824-827, 10.1038/nature09455, 2010.

Vogel, H.: The law of relation between the viscosity of liquids and the temperature., Phys. Z., 22, 645–646, 1921.

Xu, L., Suresh, S., Guo, H., Weber, R. J., and Ng, N. L.: Aerosol characterization over the southeastern United States using high-resolution aerosol mass spectrometry: spatial and seasonal variation of aerosol composition and sources with a focus on organic nitrates, Atmos. Chem. Phys., 15, 7307-7336, 10.5194/acp-15-7307-2015, 2015.

Xu, L., Pye, H. O. T., He, J., Chen, Y., Murphy, B. N. and Ng, N. L.: Experimental and model estimates of the contributions from biogenic monoterpenes and sesquiterpenes to secondary organic aerosol in the southeastern United States, Atmospheric Chemistry and Physics, 18(17), 12613–12637, doi:https://doi.org/10.5194/acp-18-12613-2018, 2018.

Yarwood, G., Whitten, G. Z., Jung, J., Heo, G. and Allen, D. T.: Development, evaluation and testing of version 6 of the Carbon Bond chemical mechanism (CB6), The University of Texas at Austin., 2010.

You, Y., Renbaum-Wolff, L., Carreras-Sospedra, M., Hanna, S. J., Hiranuma, N., Kamal, S., Smith, M. L., Zhang, X., Weber, R. J., Shilling, J. E., Dabdub, D., Martin, S. T. and Bertram, A. K.: Images reveal that atmospheric particles can undergo liquid-liquid phase separations, Proc. Natl. Acad. Sci. U.S.A., 109(33), 13188–13193, doi:10.1073/pnas.1206414109, 2012.

Yu, C. H., Zhu, X. and Fan, Z.: Spatial/Temporal Variations and Source Apportionment of VOCs Monitored at Community Scale in an Urban Area, edited by Y. Zhang, PLoS ONE, 9(4), e95734, doi:10.1371/journal.pone.0095734, 2014.

Zanobetti, A. and Schwartz, J.: The Effect of Fine and Coarse Particulate Air Pollution on Mortality: A National Analysis, Environmental Health Perspectives, 117(6), 898–903, doi:10.1289/ehp.0800108, 2009.

Zhang, H., Surratt, J. D., Lin, Y. H., Bapat, J. and Kamens, R. M.: Effect of relative humidity on SOA formation from isoprene/NO photooxidation: enhancement of 2-methylglyceric acid and its corresponding oligoesters under dry conditions, Atmospheric Chemistry and Physics, 11(13), 6411–6424, doi:https://doi.org/10.5194/acp-11-6411-2011, 2011.

Zhang, Q., Jimenez, J. L., Canagaratna, M. R., Allan, J. D., Coe, H., Ulbrich, I., Alfarra, M. R., Takami, A., Middlebrook, A. M., Sun, Y. L., Dzepina, K., Dunlea, E., Docherty, K., DeCarlo, P. F., Salcedo, D., Onasch, T., Jayne, J. T., Miyoshi, T., Shimono, A., Hatakeyama, S., Takegawa, N., Kondo, Y., Schneider, J., Drewnick, F., Borrmann, S., Weimer, S., Demerjian, K., Williams, P., Bower, K., Bahreini, R., Cottrell, L., Griffin, R. J., Rautiainen, J., Sun, J. Y., Zhang, Y. M. and Worsnop, D. R.: Ubiquity and dominance of oxygenated species in organic aerosols in anthropogenically-influenced Northern Hemisphere midlatitudes: UBIQUITY AND DOMINANCE OF OXYGENATED OA, Geophysical Research Letters, 34(13), n/a-n/a, doi:10.1029/2007GL029979, 2007.

Zhang, Y., Chen, Y., Lei, Z., Olson, N. E., Zhang, Z., Gold, A., Jayne, J. T., Worsnop, D. R., Onasch, T. B., Ault, A. P. and Surratt, J. D.: Predicting the Viscosity and pH on Inorganic-Irganic Mixed Isoprene-Derived Epoxydiols (IEPOX) aerosols, In Prep.

Zhang, Y., S. Sanchez, M., Douet, C., Wang, Y., Bateman, A., Gong, Z., Kuwata, M., Renbaum-Wolff, L., B. Sato, B., Liu, P., K. Bertram, A., Geiger, F. and T. Martin, S.: Changing shapes and implied viscosities of suspended submicron particles, Atmospheric Chemistry and Physics Discussions, 15, 6821–6850, doi:10.5194/acpd-15-6821-2015, 2015.

Zhang, Y., Chen, Y., Lambe, A. T., Olson, N. E., Lei, Z., Craig, R. L., Zhang, Z., Gold, A., Onasch, T. B., Jayne, J. T., Worsnop, D. R., Gaston, C. J., Thornton, J. A., Vizuete, W., Ault, A. P. and Surratt, J. D.: Effect of the Aerosol-Phase State on Secondary Organic Aerosol Formation from the Reactive Uptake of Isoprene-Derived Epoxydiols (IEPOX), Environ. Sci. Technol. Lett., 5(3), 167–174, doi:10.1021/acs.estlett.8b00044, 2018a.

Zhang, H., Yee, L. D., Lee, B. H., Curtis, M. P., Worton, D. R., Isaacman-VanWertz, G., Offenberg, J. H., Lewandowski, M., Kleindienst, T. E., and Beaver, M. R.: Monoterpenes are the largest source of summertime organic aerosol in the southeastern United States, Proceedings of the National Academy of Sciences, 115, 2038-2043, 2018b.

Zuend, A. and Seinfeld, J. H.: Modeling the gas-particle partitioning of secondary organic aerosol: the importance of liquid-liquid phase separation, Atmospheric Chemistry and Physics, 12(9), 3857–3882, doi:https://doi.org/10.5194/acp-12-3857-2012, 2012.

Zuend, A., Marcolli, C., Luo, B. P. and Peter, T.: A thermodynamic model of mixed organic-inorganic aerosols to predict activity coefficients, Atmospheric Chemistry and Physics, 8(16), 4559–4593, doi:https://doi.org/10.5194/acp-8-4559-2008, 2008.

https://doi.org/10.5194/acp-2019-900
Preprint. Discussion started: 7 November 2019

Tables

Table 1 - CMAQ defined aerosol phase species (Pye et al., 2017; Murphy et al., 2017) used in the calculation of the predicted organic phase parameter (overall SOA viscosity- η_{org}) and their respective organic-mass-to-organic-carbon ratio (*OM*:*OC*) (Pye et al., 2017), atomic oxygen-to-carbon ratio (*O*:*C*), molar weight (Pye et al., 2017), and predicted individual glass transition temperature (T_g) and viscosity at standard temperature.

Species Name	Description	Source	OM : OC ratio	O : C ratio	Molar weight (g/mole)	Predicted T_g (K)	Predicted η_{org} at T= 298K And ALW = 0 (Pa•s)
AALK1	SV alkane VOC SOA	ANTH	1.56	0.3146	225	256	$7.54*10^{9}$
AALK2	SV alkane VOC SOA	ANTH	1.42	0.2026	205.1	233	$5.34*10^{7}$
ABNZ1	SV High NOx SOA product from benzene	ANTH	2.68	1.2106	161	289	$1.67*10^{14}$
ABNZ2	SV High NOx SOA product from benzene	ANTH	2.23	0.8506	134	234	$2.66*10^{7}$
ABNZ3	LV low NOx SOA product from Benzene	ANTH	3.00	1.4666	180	322	$1.00*10^{12}$
AGLY	Glyoxal / methylglyoxal SOA	BIOG	2.13	0.7706	66.4	160	$1.71*10^{3}$
AISO1	SV SOA product from isoprene	BIOG	2.20	0.8266	132.0	230	$1.20*10^{7}$
AISO2	HV SOA product from isoprene	BIOG	2.23	0.8506	133.0	233	$2.26*10^{7}$

AISO3	Acid-catalyzed isoprene SOA compounds (2-methyltetrols + IEPOX organosulfate)	BIOG	2.80	1.3066	168.2	301	$1.00*10^{12}$
ALVOO1	LV Oxidized combustion organic compounds	ANTH	2.27	0.8826	136	238	$6.59*10^{7}$
ALVOO2	LV Oxidized combustion organic compounds	ANTH	2.06	0.7146	136	222	$3.97*10^{6}$
AOLGA	Oligomer products of anthropogenic SOA compounds	ANTH	2.50	1.0666	206	303	$1.00*10^{12}$
AOLGB	Oligomer products of biogenic SOA compounds	BIOG	2.10	0.7466	248	300	$1.00*10^{12}$
AORGC	Glyoxal and Methylglyoxal SOA	BIOG	2.00	0.6666	177	251	$1.33*10^{9}$
APAH1	SV High-NOx SOA product from PAHs	ANTH	1.63	0.3706	195.6	239	$1.58*10^{8}$
APAH2	SV High-NOx SOA product from PAHs	ANTH	1.49	0.2586	178.7	216	$2.80*10^{6}$
APAH3	LV low-NOx SOA product from PAHs	ANTH	1.77	0.4826	212.2	260	$1.97*10^{10}$
APCSO	Potential combustion SOA	ANTH	2.00	0.6666	170	245	$3.91*10^{8}$
ASQT	SV SOA from sesquiterpenes	BIOG	1.52	0.2826	135	179	$1.87*10^{4}$

ASVOO1	SV Oxidized combustion organic products	ANTH	1.88	0.5706	135	207	$4.69*10^5$
ASVOO2	SV Oxidized combustion organic products	ANTH	1.73	0.4506	135	195	$1.10*10^5$
ASVOO3	SV Oxidized Combustion organic compounds	ANTH	1.60	0.3466	134	184	$3.19*10^4$
AIVPO1	Intermediate Volatility Primary organic compounds	ANTH	1.17	0.0026	266	260	$3.22*10^{10}$
ALVPO1	LV Primary organic compounds	ANTH	1.39	0.1786	218	241	$2.58*10^8$
ASVPO1	SV Primary organic compounds	ANTH	1.32	0.1226	230	245	$7.00*10^8$
ASVPO2	SV primary organic compounds	ANTH	1.26	0.0746	241	249	$1.86*10^9$
ASVPO3	SV primary organic compounds	ANTH	1.21	0.0346	253	254	$6.63*10^9$
ATOL1	SV high NOx Toluene SOA	ANTH	2.26	0.8746	163	259	$8.17*10^9$
ATOL2	SV High NOx Toluene SOA	ANTH	1.82	0.5226	175	23	$7.25*10^7$
ATOL3	LV low NOx Toluene SOA	ANTH	2.70	1.2266	194	309	$1.00*10^{12}$
ATRP1	SV SOA product from monoterpenes	BIOG	1.84	0.5386	177	239	$1.30*10^8$

ATRP2	HV SOA product from monoterpenes	BIOG	1.83	0.5306	198	254	$3.93*10^{9}$
AXYL1	SV High NOx SOA product from xylene	ANTH	2.42	1.0026	174	278	$3.16*10^{12}$
AXYL2	SV High NOx SOA product from xylene	ANTH	1.93	0.6106	185	252	$1.85*10^{9}$
AXYL3	LV low-NOx SOA product from xylene	ANTH	2.30	0.9066	218	297	$1.43*10^{16}$

Table 2 - Rate constants used to calculate the effective first order rate constant for aqueous phase IEPOX SOA formation catalyzed by H^+, HSO_4^- with water and SO_4^{2-} as nucleophiles

Rate Constant	**Value (M^{-2} s^{-1})**	**Reference**
$k_{H^+,water}$	$9.00x10^{-4}$	Eddingsaas et al., 2010; Pye et al., 2013
$k_{HSO_4^-,water}$	$1.31x10^{-5}$	Eddingsaas et al., 2010
$k_{H^+,SO_4^{2-}}$	$1.27x10^{-3}$	Riedel et al. 2016; Budisulistiorini et al., 2017

Table 3 – Brief summary of different simulations conducted in this work in CMAQ v 5.2.1

Simulations	**Details**
NonPhaseSep	Base CMAQ v5.2.1 parameterization assuming homogeneous, internally mixed organic-inorganic fine aerosol, no phase separation (Pye et al., 2017)
PhaseSep	CMAQ parametrization with additional term in reactive uptake calculation to capture the impact of phase separation and organic coating described in sections 2.1-2.3 and 2.5
Emissions reduction	PhaseSep with EPA recommended emissions reductions of 34% and 48% for NO_x and SO_2 from 2013 to 2025 (See Section 2.6)
HighHorg	PhaseSep with higher organic phase Henry's law Coefficient (3 orders of magnitude higher than in PhaseSep) (See Section 2.6)
PhaseSep2	PhaseSep with the assumption that for solid or semi-solid phase Zuend and Seinfeld (2012) phase sepration criteria is followed (See Section 2.6)

Figures

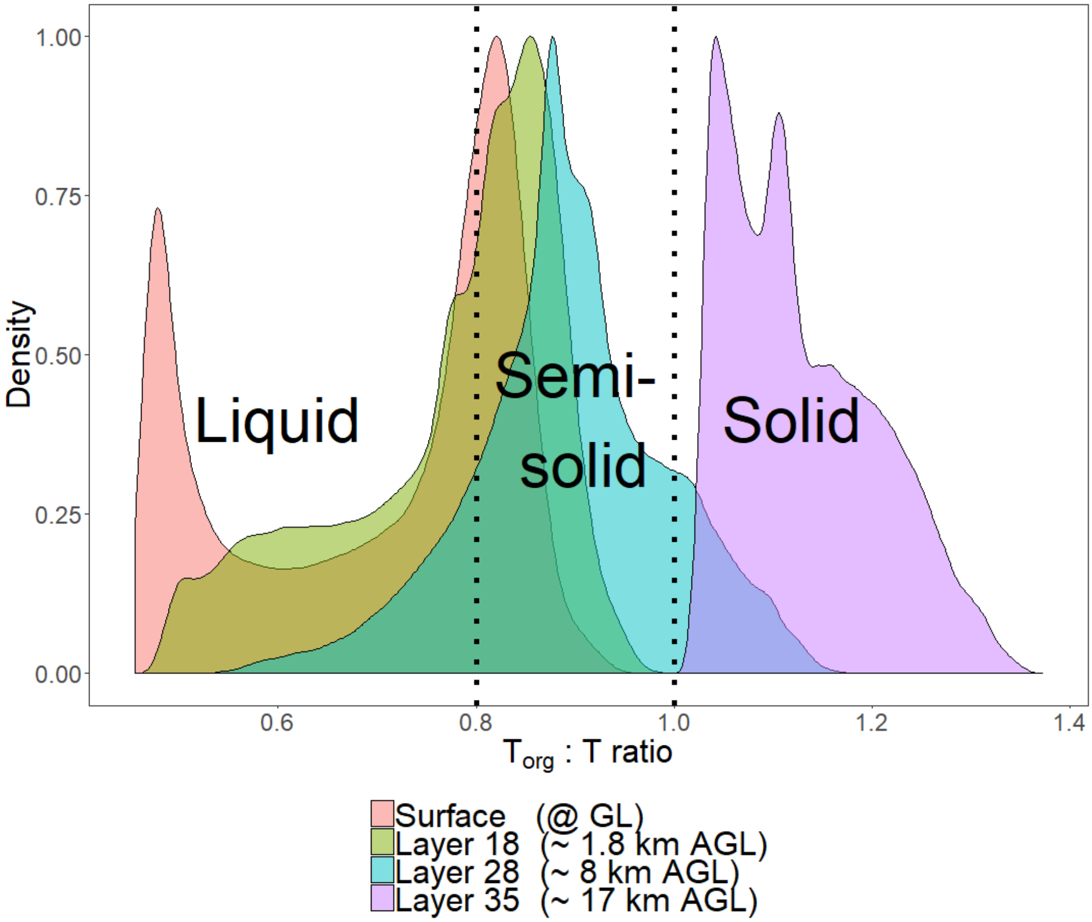

Figure 1- Probability density distribution of glass transition temperature to ambient temperature ratio (T_{org}:T) for all grid cells and time steps at the surface layer (red), 1.8 km above Surface layer (green, layer 18-lower troposphere), 8 km above Surface layer (blue, layer 28-upper troposphere) and 17 km above Surface layer (purple, layer 35-stratosphere).

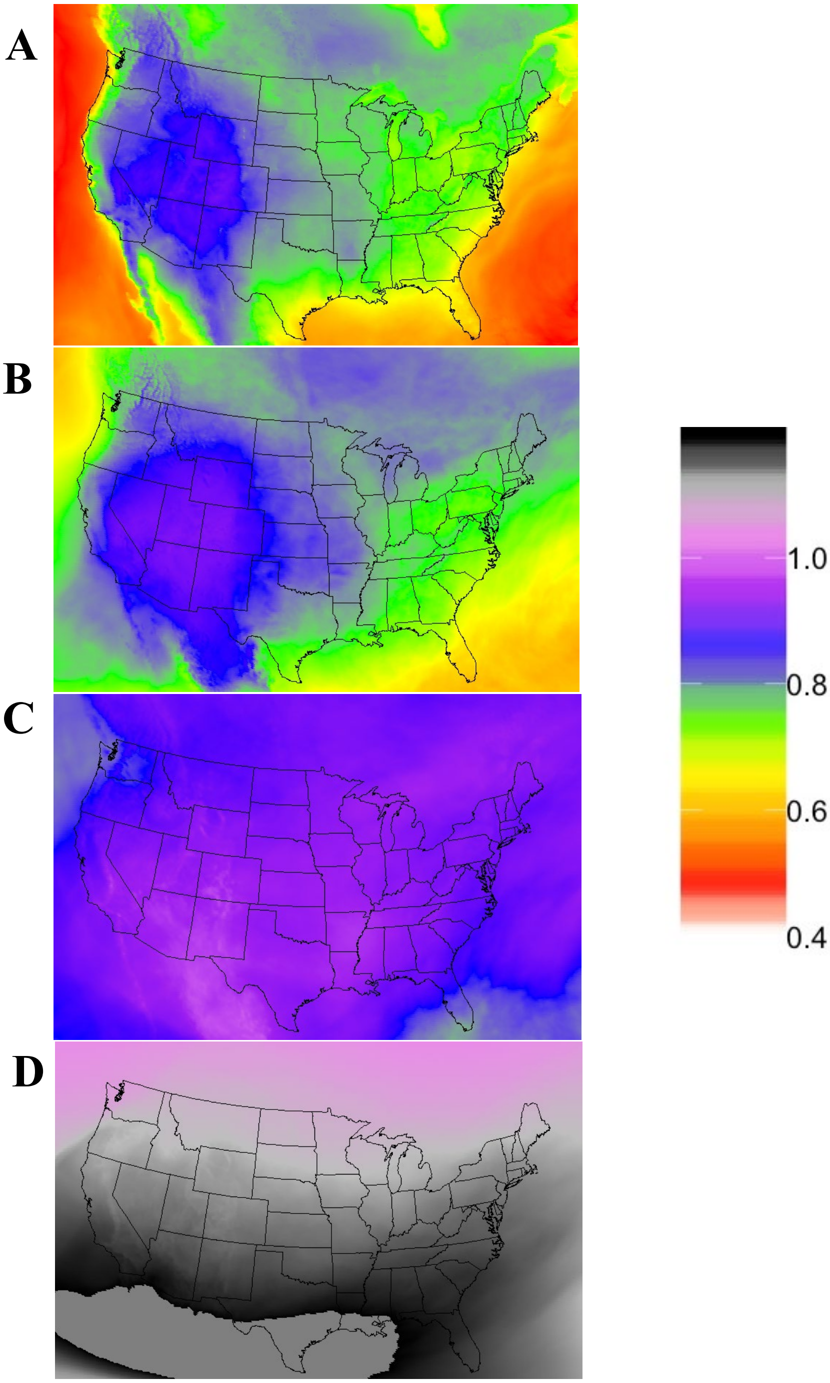
A
B
C
D
1.0
0.8
0.6
0.4

Figure 2- For all time steps and over the continental United States, the average glass transition temperature to ambient temperature (T_{org}:T) ratio at the **(A)** surface level, **(B)** 1.8 km above Surface layer (lower troposphere), **(C)** 8 km (upper troposphere) and **(D)**17 km above Surface layer (stratosphere).

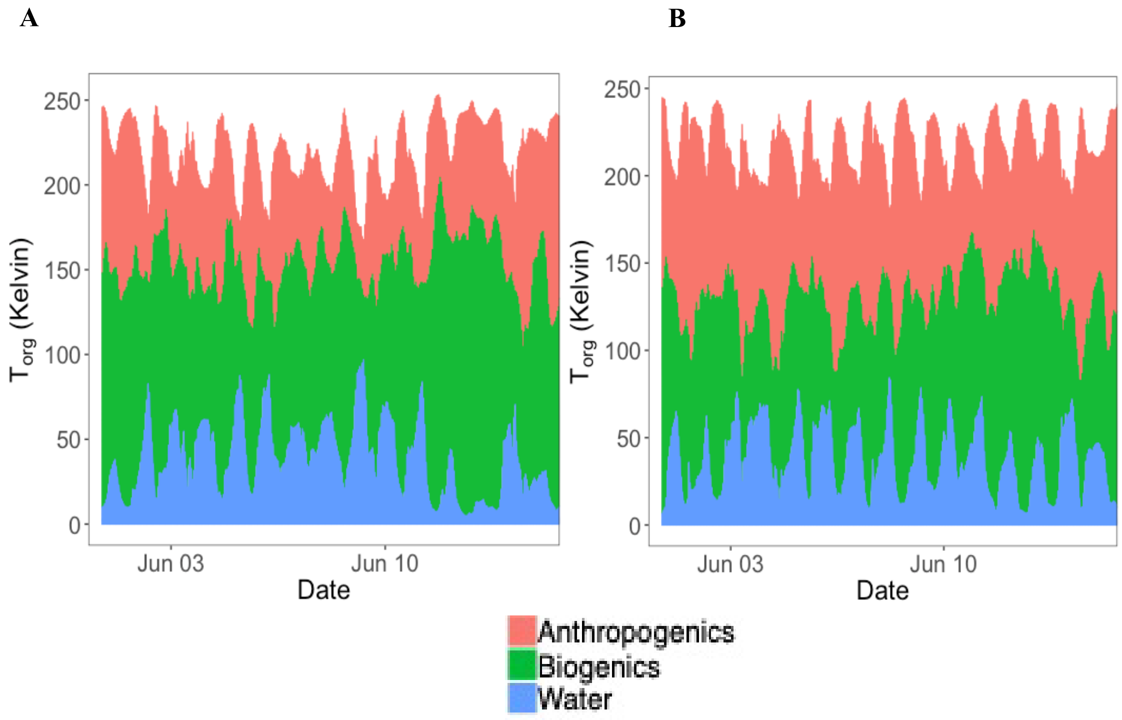

Figure 3 – From June 1 to June 15, 2013 the contributions of biogenic SOA (green), anthropogenic SOA (red), and aerosol water (blue) to glass transition temperature (T_{org}) at the **(A)** Centreville, AL site and the **(B)** Jefferson Street, Atlanta site.

https://doi.org/10.5194/acp-2019-900
Preprint. Discussion started: 7 November 2019

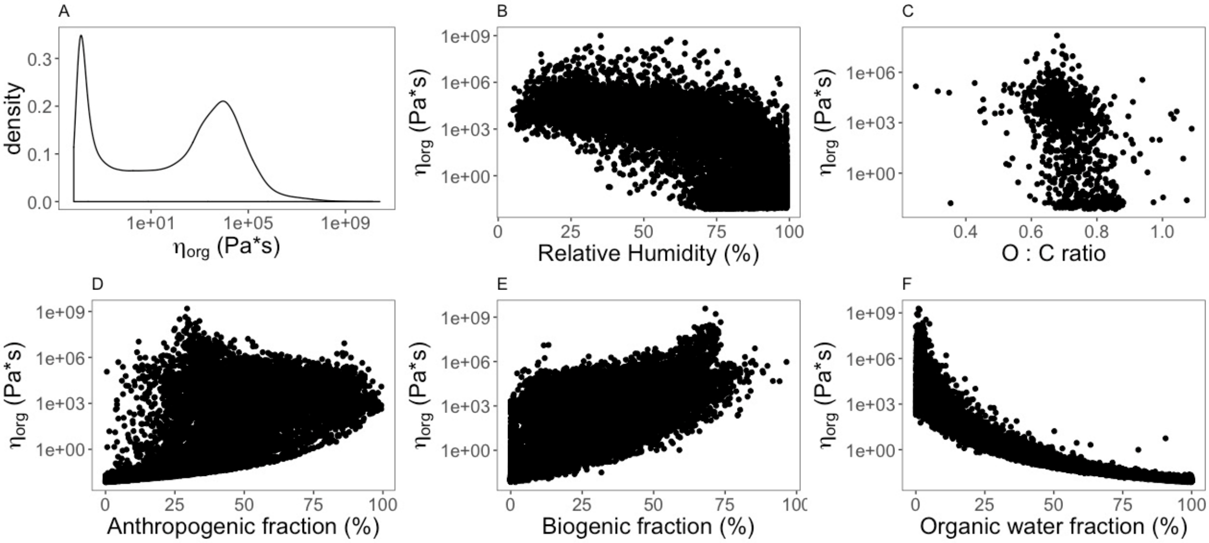

Figure 4- For all grid cells and time steps at the surface layer the (**A**) Probability distribution of the organic phase viscosity , and correlations of particle viscosity (η_{org}) with **(B)** relative humidity, **(C)** atomic oxygen-to-carbon (O:C) ratio, (**D**) anthropogenic SOA weight fraction, **(E)** biogenic SOA weight fraction and, (**F**) organic-phase water content (*ws*).

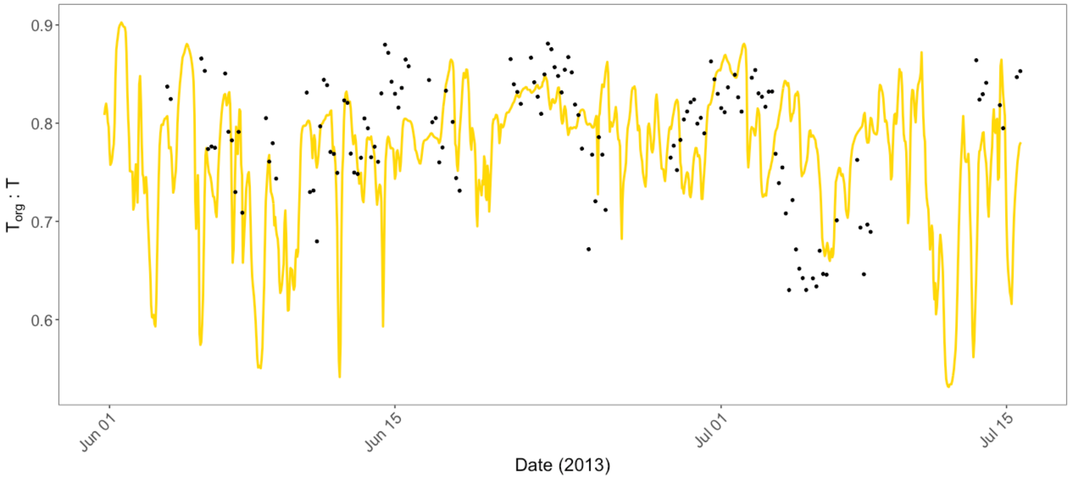

Figure 5 – Predicted glass transition temperature to ambient temperature ratio (T_{org}:T) at the Centreville, Alabama during the 2013 SOAS campaign based on OA composition reported by Zhang et al. (2018b) (black). Predicted T_{org}:T from this work is shown in yellow.

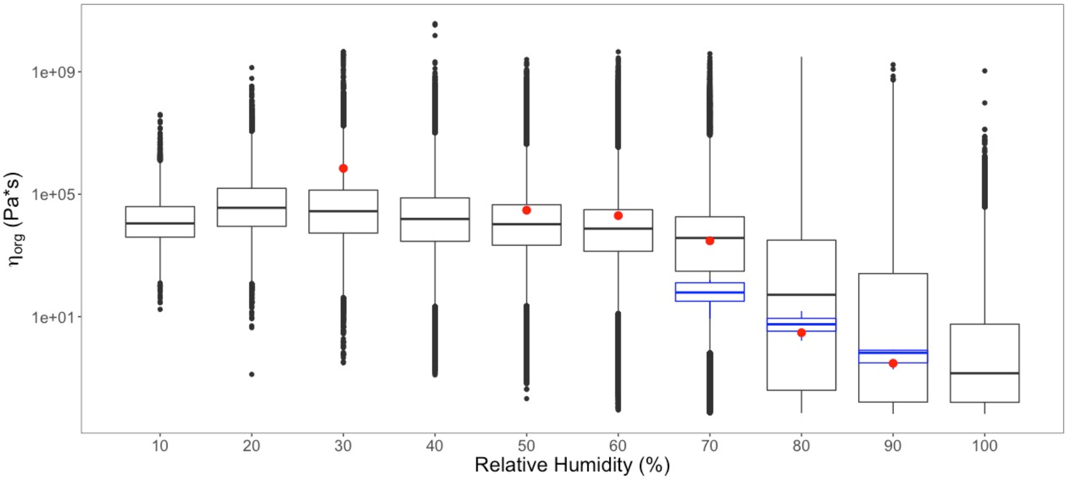

Figure 6 – Model predicted SOA viscosity (η_{org}) and experimental data for η_{org} from Zhang et al. (2018a) (red) and Song et al. (2016) (blue), at varying RH.

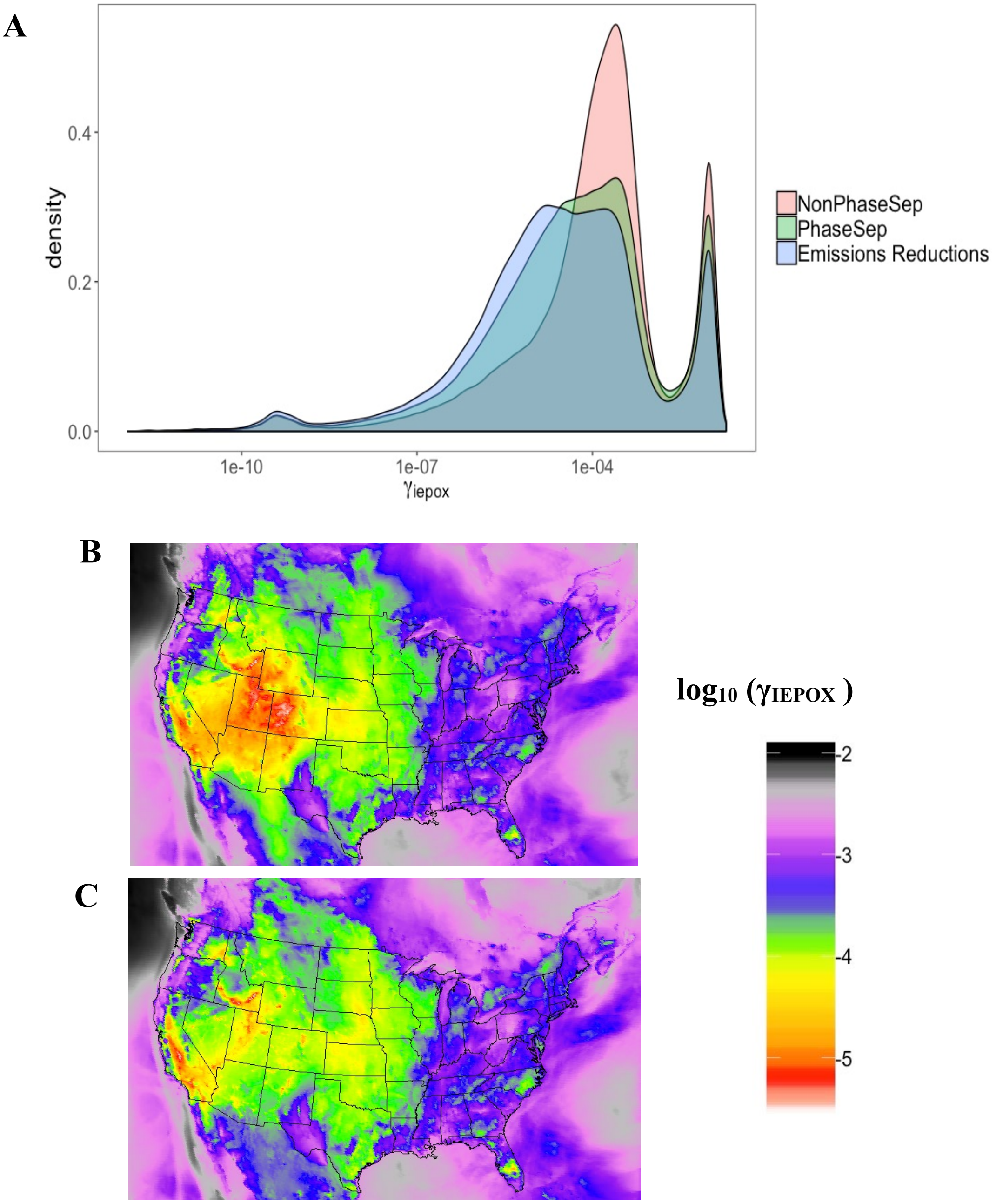
A
density
0.4
0.2
0.0
1e-10
1e-07
1e-04
γiepox
NonPhaseSep
PhaseSep
Emissions Reductions
B
C
log10 (γIEPOX)
-2
-3
-4
-5

Figure 7 – For all grid cells and time steps the predicted **(A)** probability distribution of γ_{IEPOX} at the surface level for the *NonPhaseSep* (red), *PhaseSep* (green), and *Emission reductions* (blue) simulations. For each grid cell the mean value of γ_{IEPOX} for the **(B)** *PhaseSep* simulation and **(C)** *NonPhaseSep* simulation.

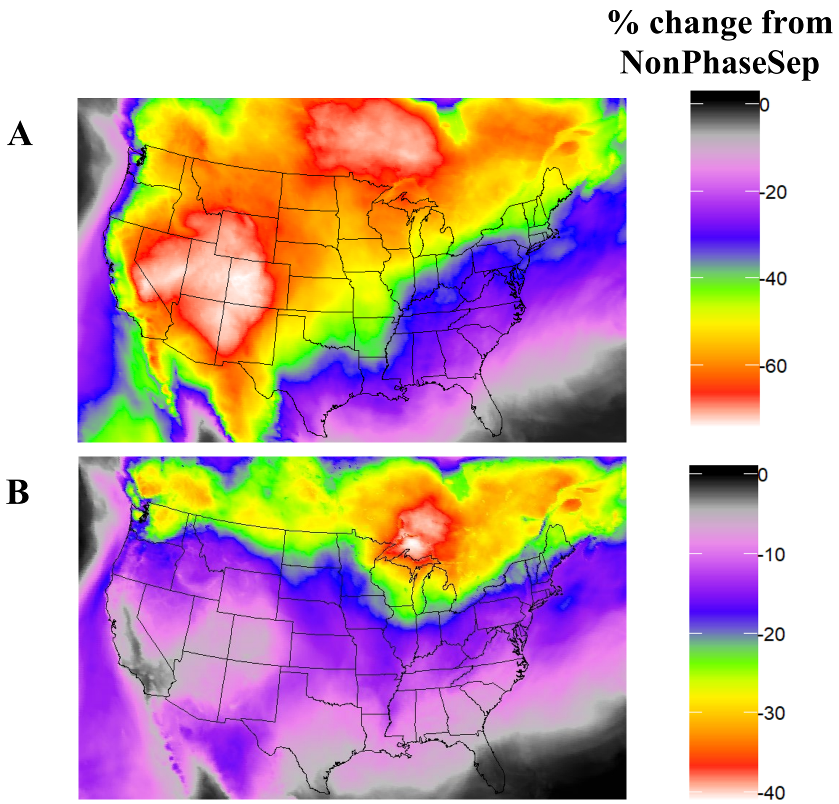

Figure 8 – Spatial map of the mean percent relative change of **(A)** IEPOX-derived SOA and **(B)** biogenic SOA mass (primarily driven by IEPOX SOA) in *PhaseSep* case relative to the *NonPhaseSep* Simulation.

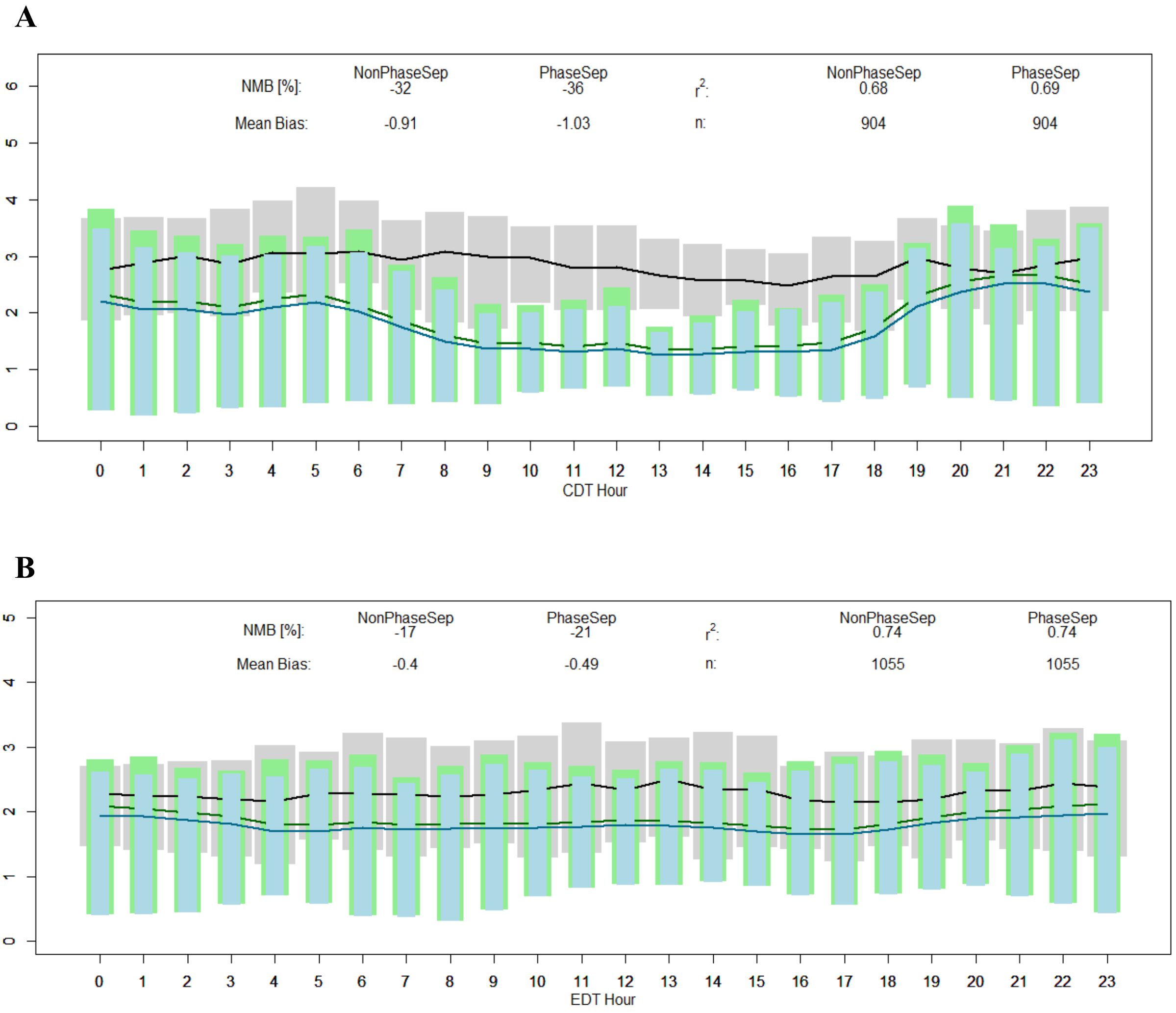

Figure 9 – $PM_{2.5}$ organic carbon (OC) mass (µg/m^3) as a function of hour of the day. Non-aggregated performance statistics- Mean Bias (µg/m^3), % Normalized Mean Bias (NMB) and Spearman's Correlation coefficient (r^2) of *NonPhaseSep* (green) and *PhaseSep* (blue) cases relative to observed (grey) $PM_{2.5}$ OC mass for **(A)** Rural Centreville, Alabama site and, **(B)** Urban

Jefferson Street, Atlanta, Georgia site. Bars/shading indicate 25th to 75th percentiles. Lines indicate means. n= number of observation points.

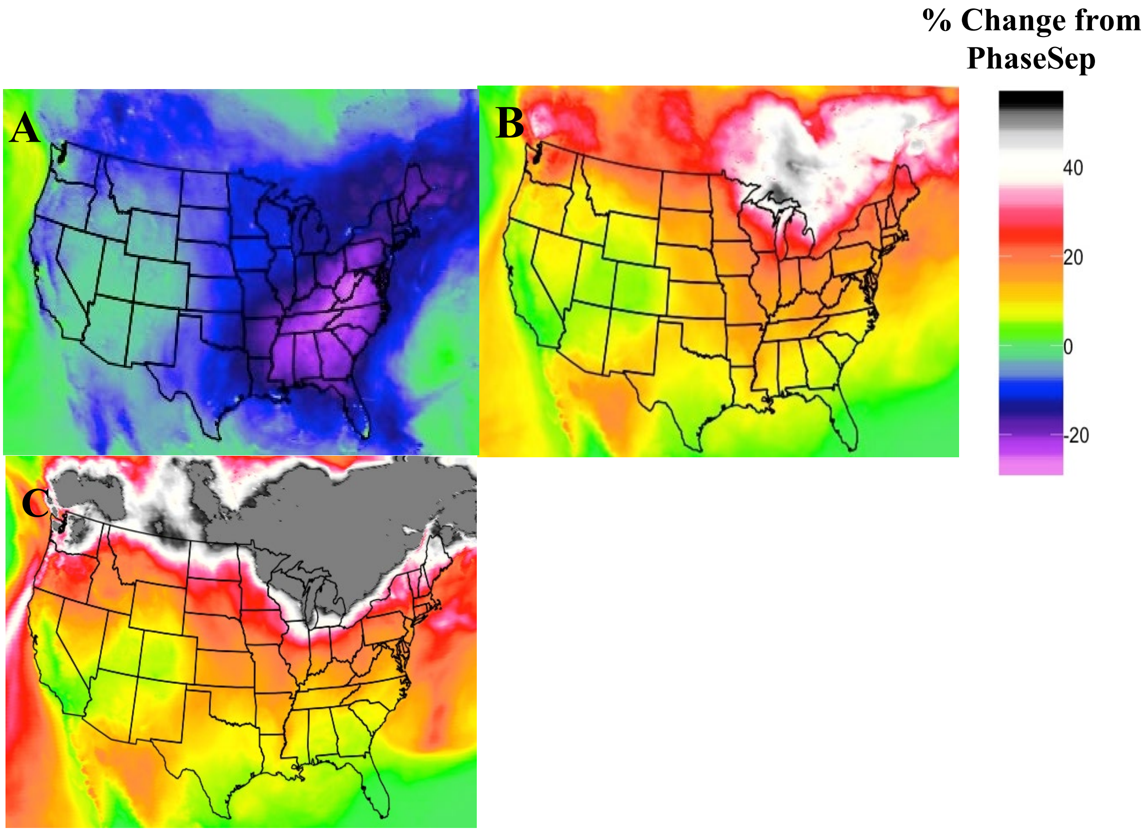

Figure 10 –Relative change (%) in biogenic SOA mass at the surface level from the PhaseSep parameterization for the **(A)** NO_x and SO_2 *emissions reduction* sensitivity simulation, **(B)** *HighHorg* sensitivity simulation, and **(C)** the *PhaseSep2* simulation that did not assume semi-solid particles were automatically phase separated.